Cleavage by signal peptide peptidase is required for the degradation of selected tail-anchored proteins

Jessica M. Boname,[1,2] Stuart Bloor,[1,2] Michal P. Wandel,[1,3] James A. Nathan,[1,2] Robin Antrobus,[1] Kevin S. Dingwell,[4] Teresa L. Thurston,[3] Duncan L. Smith,[5] James C. Smith,[4] Felix Randow,[2,3] and Paul J. Lehner[1,2]

[1]Cambridge Institute for Medical Research, University of Cambridge, Cambridge CB2 0XY, England, UK
[2]Department of Medicine, University of Cambridge, Cambridge CB2 0QQ, England, UK
[3]Division of Protein and Nucleic Acid Chemistry, Medical Research Council Laboratory of Molecular Biology, Cambridge CB2 0QH, England, UK
[4]Medical Research Council National Institute for Medical Research, London NW7 1AA, England, UK
[5]Cancer Research UK Manchester Institute, University of Manchester, Manchester M20 4B, England, UK

The regulated turnover of endoplasmic reticulum (ER)–resident membrane proteins requires their extraction from the membrane lipid bilayer and subsequent proteasome-mediated degradation. Cleavage within the transmembrane domain provides an attractive mechanism to facilitate protein dislocation but has never been shown for endogenous substrates. To determine whether intramembrane proteolysis, specifically cleavage by the intramembrane-cleaving aspartyl protease signal peptide peptidase (SPP), is involved in this pathway, we generated an SPP-specific somatic cell knockout. In a stable isotope labeling by amino acids in cell culture–based proteomics screen, we identified HO-1 (heme oxygenase-1), the rate-limiting enzyme in the degradation of heme to biliverdin, as a novel SPP substrate. Intramembrane cleavage by catalytically active SPP provided the primary proteolytic step required for the extraction and subsequent proteasome-dependent degradation of HO-1, an ER-resident tail-anchored protein. SPP-mediated proteolysis was not limited to HO-1 but was required for the dislocation and degradation of additional tail-anchored ER-resident proteins. Our study identifies tail-anchored proteins as novel SPP substrates and a specific requirement for SPP-mediated intramembrane cleavage in protein turnover.

Introduction

The homeostasis of proteins in the ER is highly dependent on effective quality control pathways that recognize and dispose of proteins that are either misfolded or surplus to requirement (Hegde and Ploegh, 2010; Brodsky, 2012). The ER-associated degradation (ERAD) pathway promotes the dislocation of proteins from the ER into the cytosol, where they can be degraded by the proteasome. ERAD therefore plays an important role in maintaining homeostasis within the early secretory pathway.

The established requirements for ERAD are the recognition, ubiquitination, and dislocation of proteins across the ER membrane, although mechanistic insight into this process is still required (Vashist and Ng, 2004; Carvalho et al., 2006). A core component of the cellular ERAD machinery is a membrane-embedded ER ligase, which, either directly or with the aid of luminal adaptors, binds ERAD substrates (Kostova et al., 2007). In yeast, two ERAD E3 ligases, Hrd1p and Doa10p, are sufficient to recognize the diverse set of misfolded proteins (Mehnert et al., 2010), whereas in mammals, the repertoire of ERAD E3 ligases has diversified (Li et al., 2008), presumably to cope with the higher degree of specialization and regulation required in complex multicellular organisms.

Viruses also appropriate cellular ERAD pathways to degrade host proteins. Two well-characterized viral gene products from human cytomegalovirus, US2 and US11, hijack separate ERAD pathways to degrade newly synthesized major histocompatibility complex (MHC) class I (MHC-I) molecules (Wiertz et al., 1996a,b;

J.M. Boname and S. Bloor contributed equally to this paper.

Correspondence to Paul J. Lehner: pjl30@cam.ac.uk

Abbreviations used in this paper: ERAD, ER-associated degradation; MHC, major histocompatibility complex; SILAC, stable isotope labeling by amino acids in cell culture; SP, signal peptidase; SPP, signal peptide peptidase; TMD, transmembrane domain; WT, wild type.

The Rockefeller University Press $30.00
J. Cell Biol. Vol. 205 No. 6 847–862
www.jcb.org/cgi/doi/10.1083/jcb.201312009

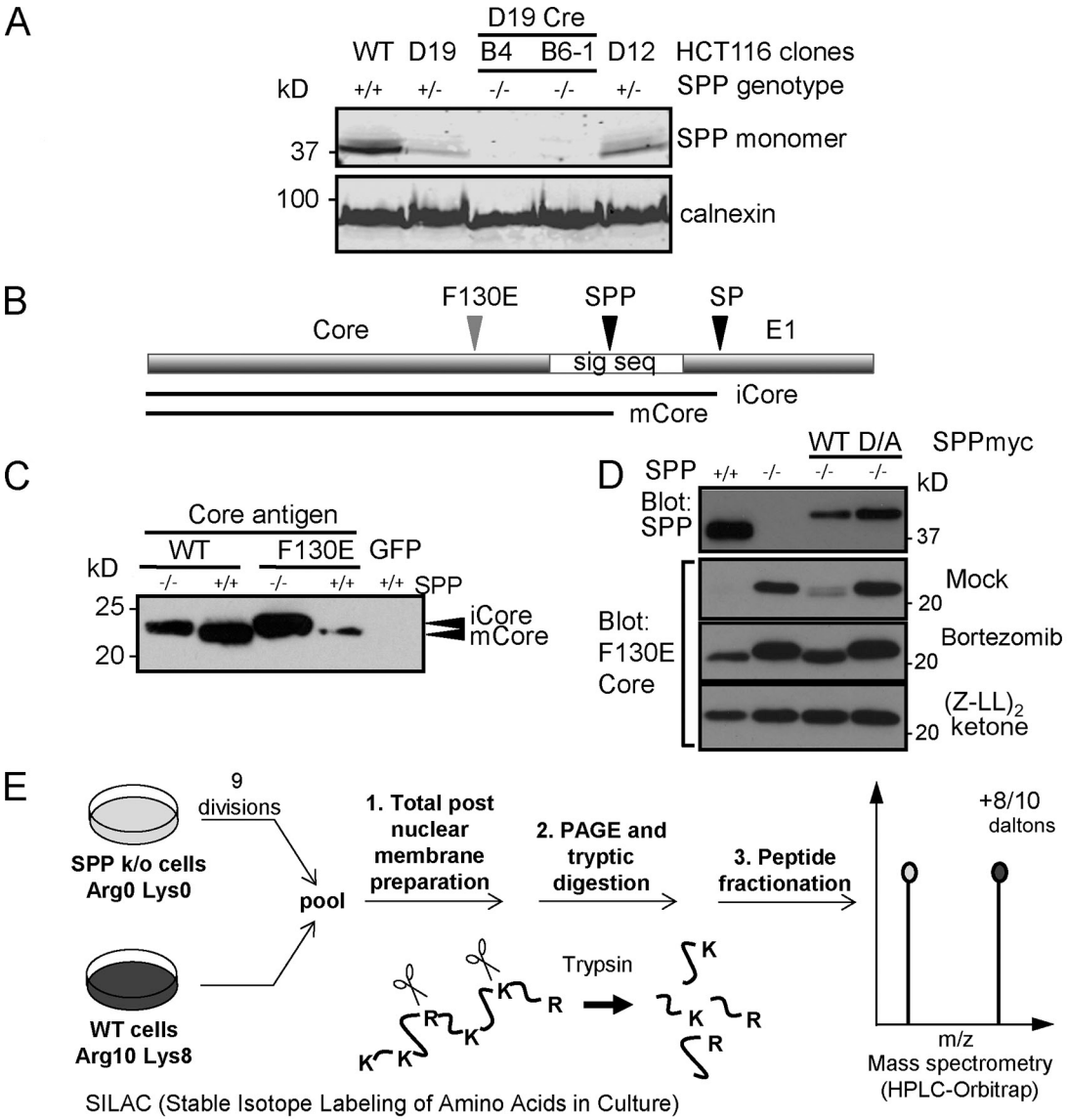

F

		Reverse SILAC		Forward SILAC		RNAseq Analysis	
Protein name	**UniProt**	**B4/ WT**	**Pep**	**1/(WT/ B4)**	**Pep**	**Gene name**	**Log Fold Change**
Signal peptidase complex catalytic subunit SEC11C	**Q9BY50**	**4.12**	**1**	**5.26**	**1**	**SEC11C**	**<± 0.4**
Cell cycle progression restoration protein 2	Q969Z0-1	2.35	3	2.12	2	TBRG4	2.59
Heme oxygenase 1	**P09601**	**2.05**	**9**	**2.27**	**9**	**HMOX1**	**<± 0.4**
Endoplasmic reticulum stress-response protein 25	Q7Z7H5-1	2.07	3	2.22	4	TMED4	<± 0.4
Protein YIPF2	Q9BWQ6	1.97	1	2.22	1	YIPF2	<± 0.4
ATP-binding cassette subfamily B member 6	Q9NP58-1	2.13	6	2.27	6	ABCB6	<± 0.4
CD98 Light chain	Q01650	0.49	4	0.58	3	SLC7A5	<± 0.4
Long-chain acyl-CoA synthetase 5	Q9ULC5-3	0.50	15	0.40	13	ACSL5	<± 0.4
Signal peptide peptidase	Q8TCT9-1	-	5	-	2	HM13	See Fig. S3

Figure 1. **A functional proteomics screen in a SPP somatic cell knockout identifies HO-1 as a potential SPP substrate.** (A) Odyssey infrared capture of immunoblot for SPP on SPP wild-type (WT, +/+) HCT116, SPP heterozygous (D19 and D12, +/−), or SPP knockout (B4 and B6-1, −/−). (B) Schematic of core/E1 hepatitis C polyprotein expressed from a lentivirus, with signal peptidase (SP) and signal peptide peptidase (SPP) cleavage sites (black arrowheads). The site of the F130E mutation within the amphipathic helix of core is noted (gray arrowhead). The immature (iCore) and mature (mCore) core products, produced after SP and SPP cleavage, are also shown. sig seq, signal sequence. (C) Immunoblot for core antigen in cells expressing WT or mutant (F130E) core in WT (+/+) or SPP knockout (−/−) cells. (D) Immunoblot for mutant (F130E) core antigen in WT (+/+), SPP knockout (−/−), or SPP knockout

Lilley and Ploegh, 2005). The study of US2 and US11 has led to the identification of novel ERAD components and helped define the ERAD pathway in mammalian cells (Lilley and Ploegh, 2005). In a genetic screen, we recently identified TRC8, an ER-resident, polytopic membrane protein, as the E3 ligase required for the US2-mediated ubiquitination and dislocation of MHC-I molecules (Stagg et al., 2009). We found that in both the presence and absence of US2, TRC8 readily associated with the intramembrane-cleaving aspartyl protease signal peptide peptidase (SPP), an enzyme previously implicated in the US2-mediated dislocation of MHC-I (Loureiro et al., 2006). This association of SPP with TRC8 was intriguing, not least because of the potential role for intramembrane proteolysis in the cleavage and dislocation of membrane proteins en route from the ER to the cytosol. SPP cleaves substrate polypeptides in their transmembrane domain (TMD) and has two active site aspartate residues within the conserved motifs YD and LGLGD of adjacent membrane-spanning regions (Lemberg and Martoglio, 2004; Golde et al., 2009). The orientation of these active sites of SPP within the transmembrane regions is inverted relative to the closely related presenilin proteases (Weihofen et al., 2002), with the important functional consequence that presenilins cleave membrane proteins with a type I orientation, whereas SPP only cleaves membrane proteins with a type II orientation, a conserved feature of all known SPP substrates. The best-characterized function of SPP is the intramembrane cleavage of signal sequence stubs left in the ER membrane after signal peptidase (SP)–mediated processing of the precursor protein. Proteolytic cleavage by SPP promotes the release of these signal peptide fragments into the cytosol. In a similar fashion, SPP is required for maturation of the hepatitis C virus core protein (McLauchlan et al., 2002).

While the activity of SPP in liberating signal peptides from the ER membrane is well characterized, whether SPP plays a significant role in the degradation of endogenous ER proteins is unclear. Although SPP-mediated cleavage of an ERAD substrate has not been reported, a role for intramembrane proteolysis in ER protein degradation is attractive, as cleavage within the plane of the membrane will reduce the energy required for dislocation and thereby facilitate extraction of the protein from the membrane (Greenblatt et al., 2012). Fragments of ERAD substrates have in fact been identified in the cytosol after proteasome inhibition (Huppa and Ploegh, 1997; Loo and Clarke, 1998), but this is not a general requirement for ERAD, as full-length deglycosylated ERAD substrate intermediates, e.g., MHC-I molecules (Blom et al., 2004), can be identified in the cytosol. The finding that several critical ERAD components (Derlins, UBAC2, and iRhoms) are themselves inactive homologues of the rhomboid family of intramembrane-cleaving serine proteases (Greenblatt et al., 2011; Zettl et al., 2011; Christianson et al., 2012) lends support to the idea that dislocation and proteolysis may share common underlying mechanistic features. RHBDL4, an ER-resident, intramembrane-cleaving, active rhomboid protease, promotes ERAD by cleaving type I transmembrane proteins (TCR-α) as well as polytopic membrane proteins (mutant opsin and mutant polycystin-1; Fleig et al., 2012). Expression of RHBDL4 increases with ER stress, which, together with the identification of an ubiquitin-interacting motif in the cytosolic tail, supports a potential role for RHBDL4 in ERAD, though endogenous ERAD substrates have not been identified.

To further investigate the role of intramembrane-cleaving proteases, in particular SPP, in the cleavage and dislocation of ERAD substrates, we generated a somatic cell knockout of SPP. Using a functional proteomics approach, we here identify a critical role for SPP in the proteolytic cleavage and subsequent dislocation and degradation of endogenous HO-1 (heme oxygenase-1), a tail-anchored ER-resident protein, which is the rate-limiting enzyme in the degradation of heme to biliverdin and carbon monoxide. This SPP activity is not limited to HO-1 but is required for the dislocation and degradation of additional tail-anchored ER-resident proteins.

Results

A functional proteomics screen identifies a role for SPP in the degradation of the tail-anchored protein HO-1

We recently identified TRC8 as the ubiquitin E3 ligase recruited by human cytomegalovirus–encoded US2 for the ERAD of MHC-I molecules. TRC8 is an ER-resident E3 ligase, which we found to associate with the intramembrane-cleaving aspartyl protease SPP, suggesting a potential role for this protease in the ERAD of client substrate proteins (Stagg et al., 2009). To determine whether SPP plays a role in the dislocation of proteins from the ER membrane into the cytosol, we generated a conditional knockout of SPP in the epithelial colorectal carcinoma cell line HCT116. LoxP-flanking sites were engineered into one of the two targeting constructs, which allowed for its later removal after introduction of Cre recombinase (Figs. S1 and S2 and Tables S1–S3).

Targeted deletion of a single SPP allele significantly reduced SPP protein levels, as detected by immunoblot analysis (Fig. 1 A, clones D19/D12). Subsequent treatment of these cells with Cre recombinase successfully deleted the remaining SPP allele, resulting in a complete loss of SPP protein (Fig. 1 A, clones B4/B6-1). $SPP^{-/-}$ cells appeared healthy but grew slightly slower and were less adherent compared with parental cells. To confirm that the genetic absence of SPP caused the predicted phenotype, we tested whether $SPP^{-/-}$ cells cleave and release the hepatitis

(−/−) cells transduced with exogenous SPP WT or catalytically inactive SPP D/A mutant, in the presence of mock (top), proteasome (Bortezomib; middle), or the SPP-specific $(Z\text{-}LL)_2$ ketone (bottom) inhibitors. (E) Schematic of SILAC mass spectrometry procedure. The experiment was performed in forward and reverse labeling. k/o, knockout; m/z, mass per charge. (F) Results of RNA-Seq analysis for these proteins are also listed. In the reverse SILAC experiment, SPP WT HCT116 cells were cultured in light SILAC media (L), and in the forward experiment, SPP WT HCT116 cells were cultured in heavy SILAC media (H). Reported SILAC ratios in the reverse analysis are H/L, i.e., B4 cells/HCT116 WT cells and, in the forward analysis, are 1/(H/L), i.e., 1/(HCT116 WT cells/B4 cells). Pep represents the unique peptide count. The proteins highlighted in bold type are of type II orientation (either transmembrane or tail anchored). SPP-derived peptides were only identified from SPP HCT116 WT cells and not from SPP knockout B4 cells.

C core antigen, a well-established SPP substrate (McLauchlan et al., 2002). The hepatitis C polyprotein is cotranslationally inserted into the ER membrane. Initial cleavage of the N-terminal core antigen (core) by signal peptidase leaves the immature core in the ER membrane. Subsequent intramembrane cleavage by SPP promotes the release of mature core from the ER membrane, allowing its insertion into lipid droplets via an amphipathic helix (Fig. 1 B; Boulant et al., 2006; McLauchlan, 2009). By gel electrophoresis, wild-type (WT) core migrated slower in the SPP knockout ($SPP^{-/-}$) cell line as compared with the WT SPP ($SPP^{+/+}$) parental cell line, consistent with a loss of SPP-mediated cleavage (Fig. 1 C, first and second lanes). The difference between $SPP^{-/-}$ and WT cells was readily detected on examination of a mutant hepatitis C virus core, in which a single F130E substitution breaks the amphipathic helix and prevents insertion of core into lipid droplets (Boulant et al., 2006). As reported, the F130E core was rapidly degraded in WT SPP cells (Fig. 1 C, fourth lane). In contrast, the F130E core was stably expressed in SPP knockout cells (Fig. 1 C, third lane), presumably because it could not be extracted from the ER membrane. Genetic complementation of SPP knockout cells with WT SPP restored normal function (Fig. 1 D). The F130E hepatitis C core mutant was rapidly degraded after reintroduction of WT SPP but not the catalytically inactive D265A mutant (D/A; Fig. 1 D, second blot, third and fourth lanes, respectively). Degradation of F130E core was protected by both proteasome (bortezomib) and SPP-specific ($(Z\text{-}LL)_2$ ketone) inhibitors. As predicted, bortezomib rescued a faster migrating, cleaved form of F130E core (Fig. 1 D, third blot, first and third lanes), whereas treatment with the SPP inhibitor protected the slower migrating, uncleaved F130E core band (Fig. 1 D, fourth blot, first and third lanes). We therefore conclude that $SPP^{-/-}$ cells behave as phenotypic and functional SPP knockouts.

We were concerned that the SPP knockout cells may have compensated for the complete absence of SPP and up-regulated one or more related intramembrane-cleaving proteases. However, these were not detected by proteomic (Fig. 1 F) or RNA-Seq analysis of SPP WT and deficient cells (Table S4). Specifically, we found no change in the level of the related ER-resident SPPL3 nor did we see any change in transcript levels for the related proteases SPPL2A, SPPL2B, ADAM10, or DERLIN1. In addition, the RNA-Seq confirmed the loss of exon 3 of HM13 in the knockout cell line (Fig. S3).

To identify potential SPP substrates, we performed a proteomic screen to isolate ER membrane proteins that accumulate in SPP knockout cells. The rationale was that SPP substrates should accumulate in the ER membrane of SPP knockout cells. Using a stable isotope labeling by amino acids in cell culture (SILAC)–based functional proteomics technique (Mann, 2006), we compared the relative abundance of microsomal proteins between SPP WT and SPP knockout cell lines (Fig. 1 E). The experiment was performed in forward and reverse conditions, swapping the heavy and light isotope label between experiments. The validity of this experimental approach was confirmed as SPP-derived peptides were identified in the WT but not in the SPP knockout cells. (Fig. 1 F). Six membrane proteins were up-regulated more than twofold in the absence of SPP, of which only two were in a type II membrane orientation required for cleavage by SPP; Sec11c (see Fig. 3 B) and heme oxygenase (HO-1), the well-characterized rate-limiting enzyme that catalyzes the degradation of heme to biliverdin and carbon monoxide (Ryter et al., 2006).

Endogenous HO-1 is degraded in an SPP-dependent pathway

To validate the mass spectrometry data, we probed for endogenous HO-1 by immunoblot analysis of SPP WT and SPP knockout total cell lysates. The HO-1 antibody was insufficiently sensitive to visualize basal levels of HO-1 in either WT or SPP knockout cells (Fig. 2 A). However, endogenous HO-1 can be induced by several physiological stimuli and was readily detected after incubation of cells with 50 µM hemin for 15 h (Fig. 2 A). Subsequent removal of hemin allowed us to follow the degradation of endogenous HO-1 and determine whether SPP was required for its degradation. In SPP knockout cells, HO-1 degradation was delayed, as compared with WT, best seen at 12 and 24 h after hemin induction (Fig. 2 A). This delay in degradation could be rescued by exogenous expression of WT SPP (Fig. 2 B), suggesting a role for SPP in HO-1 degradation. Furthermore, the catalytically inactive SPP D265A (SPP D/A) mutant had a dominant-negative effect and stabilized HO-1 (Fig. 2 B), presumably through the formation of inactive enzyme–substrate complexes.

As a result of concerns that the SPP knockout cells had compensated for the prolonged absence of SPP, we took an alternative, RNAi-mediated approach to determine whether short-term depletion of SPP also affected HO-1 degradation. We used siRNA to deplete SPP from HeLa cells, induced HO-1 expression with hemin, and after removal of this stimulus, monitored HO-1 degradation over time. The rate of endogenous HO-1 degradation was dramatically reduced in SPP-depleted HeLa cells (Fig. 2 C), with an estimated half-life of 10 h from the peak of HO-1 induction (Fig. 2 C, bottom). 24 h after removal of hemin, HO-1 levels had almost completely degraded in WT cells, with little HO-1 degradation from SPP-depleted cells. In conclusion, our experiments from both SPP knockout as well as SPP-depleted cells identify a critical role for SPP in the degradation of endogenous HO-1.

SPP-mediated intramembrane cleavage is required for HO-1 dislocation and degradation

To further determine the cellular requirements for HO-1 degradation, we examined endogenous HO-1 degradation in the HEK-293T cell line. As seen in HCT116 and HeLa cells, detection of endogenous HO-1 in HEK-293T cells required induction with hemin (Fig. 3 A). After removal of the hemin stimulus, HO-1 degradation was inhibited by incubation with either the proteasome inhibitor lactacystin or the SPP-specific inhibitor $(Z\text{-}LL)_2$ ketone (Fig. 3 A). Overexpression of WT SPP induced the rapid degradation of HO-1 (Fig. 3 B), whereas the catalytically inactive (SPP D/A) mutant again showed a dominant-negative effect and stabilized HO-1 expression. In contrast, levels of exogenous Sec11c were not affected by overexpression of WT SPP (Fig. 3 B). Although HO-1 binding to WT SPP was not detected as a result

of rapid HO-1 degradation, we took advantage of the stabilization of HO-1 by the SPP D/A mutant to demonstrate binding of HO-1 to SPP (Fig. 3 C). Immunoprecipitation of HA–HO-1 allowed detection of the SPP D/A mutant (Fig. 3 C, left), and the reciprocal pull-down of myc-SPP D/A detected HA–HO-1 (Fig. 3 C, middle), confirming the interaction between these proteins.

Having demonstrated a requirement for SPP catalytic activity in HO-1 degradation, we wanted to determine whether HO-1 was itself a direct substrate. To visualize progression of HO-1 degradation, we performed a pulse–chase analysis of [^{35}S]methionine/cysteine-radiolabeled cells and immunoprecipitated HA-tagged HO-1. After overexpression of WT or catalytically inactive SPP (SPP D/A), HO-1 can be visualized in both the cleaved and uncleaved form (Fig. 4 A). The dominant-negative activity of the SPP D/A mutant was confirmed, as it stabilizes uncleaved HO-1, detected as a single band (Fig. 4 A, third and fourth lanes). In contrast, upon overexpression of WT SPP, HO-1 is already detected in a predominantly cleaved form at the 0-h time point, with a very faint, more slowly migrating uncleaved form corresponding to the single band seen with the SPP D/A mutant (Fig. 4 A, first lane). By the 2-h chase point, only the cleaved, faster migrating band remains detectable and has lost intensity compared with the 0-h time point at the start of the chase (Fig. 4 A, second lane). The small change in molecular mass corresponds to the predicted loss of an ∼10–amino acid polypeptide fragment of HO-1 after SPP cleavage (Fig. 4 A, compare first and second lanes with third and fourth lanes) by WT but not the SPP D/A mutant.

To improve resolution of these subtle changes in band migration and visualize the proteolytic HO-1 intermediates more clearly, a truncation mutant, HO-1Δ30–184 (HO-1 short), was generated. Pulse/chase analysis revealed a similar result to that seen with full-length HO-1: in the presence of the SPP D/A mutant, a single slower migrating band representing the uncleaved form of HO-1 short (Fig. 4 B, third and fourth lanes) was detected. This band remained stable over the time course of the chase. In the presence of WT SPP, an HO-1 precursor product relationship was again seen. At the start of the chase (Fig. 4 B, first lane) both cleaved and uncleaved forms of HO-1 were detected, and by the 1-h chase point, both fragments had lost intensity, with only the faster migrating, cleaved form of HO-1 remaining visible (Fig. 4 B, second lane). We conclude that HO-1 is a substrate of SPP and HO-1 cleavage is required for its degradation.

To determine whether SPP cleavage of substrate (HO-1) precedes its extraction from the ER membrane, and subsequent proteasome-dependent degradation, we separated cells from a pulse–chase experiment into membrane pellets and soluble fractions, in the presence or absence of lactacystin (Fig. 4 C). In the presence of WT SPP, cleavage and release of HO-1 into the soluble fraction was proteasome independent, but the cleaved form of HO-1 was degraded in a proteasome-dependent pathway. In contrast, the SPP D/A mutant stabilized the uncleaved higher molecular mass HO-1 polypeptide, which accumulated in the membrane fraction and was not released into the soluble cytosolic fraction. Collectively, these experiments demonstrate an absolute requirement for SPP catalytic activity for the cleavage and subsequent extraction of HO-1 from the lipid bilayer into the cytosol for proteasome-dependent degradation.

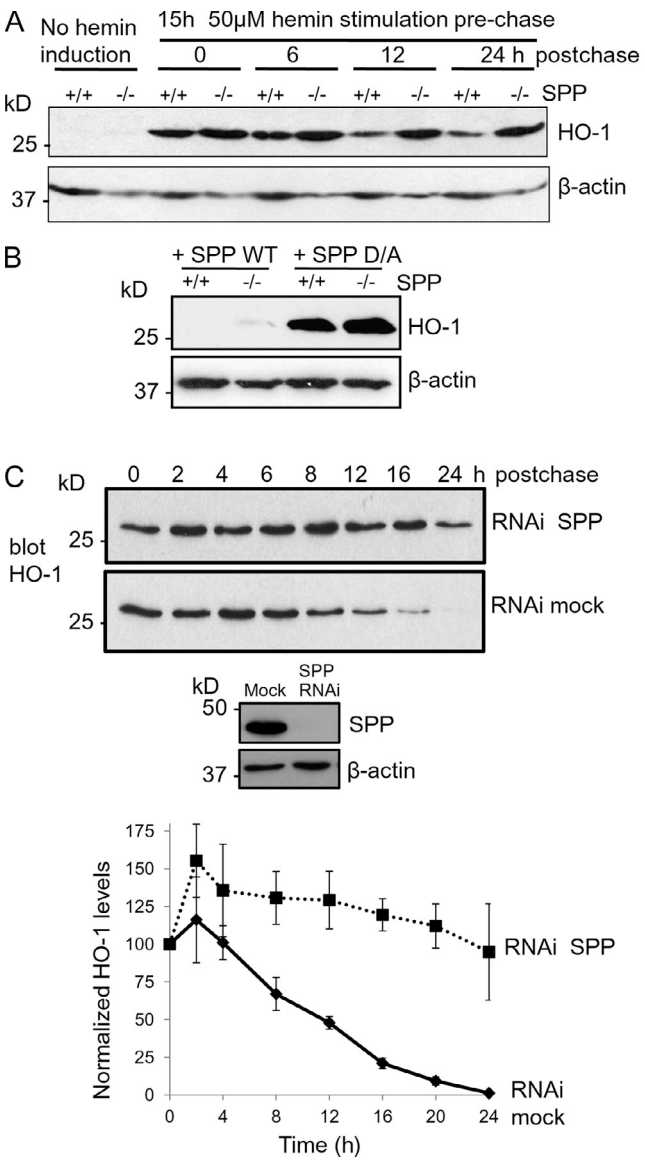

Figure 2. **Endogenous HO-1 is degraded in an SPP-dependent pathway.** (A–C) Immunoblot for HO-1. (A) WT (HCT116$^{+/+}$) and SPP knockout (B4$^{-/-}$) cells were treated with 50 µM hemin (+) for 15 h to induce HO-1. Hemin was removed, and cells were harvested at the times indicated (0/6/12/24 h after hemin induction), using β-actin as a loading control. Cycloheximide was added to all samples after hemin removal to block de novo protein synthesis. (B) WT (HCT116$^{+/+}$) and SPP knockout (B4$^{-/-}$) cells were complemented by overexpression of either SPP WT– or SPP D/A–expressing vectors. The complemented cells were harvested 24 h after hemin induction and blotted for HO-1. (C) SPP RNAi– or mock-transfected HeLa cells were treated with 50 µM hemin for 20 h to induce HO-1. Hemin was removed, and cells were harvested at the times indicated after hemin induction (hours postchase) and blotted for HO-1. Cycloheximide was added to all samples after hemin removal to block de novo protein synthesis. Inset shows depletion of SPP at $t = 0$ h. The chart at the bottom represents the quantification of three independent mock and SPP RNAi transfections. Scanned images were quantified using ImageJ v.1.46r (National Institutes of Health; Schneider et al., 2012). HO-1 levels are normalized against β-actin levels. The error bars represent the standard error.

Selected ER-resident tail-anchored proteins are cleaved and degraded in an SPP-dependent fashion

To determine whether SPP-mediated cleavage was unique to HO-1 or required for the degradation of other ER-resident tail-anchored

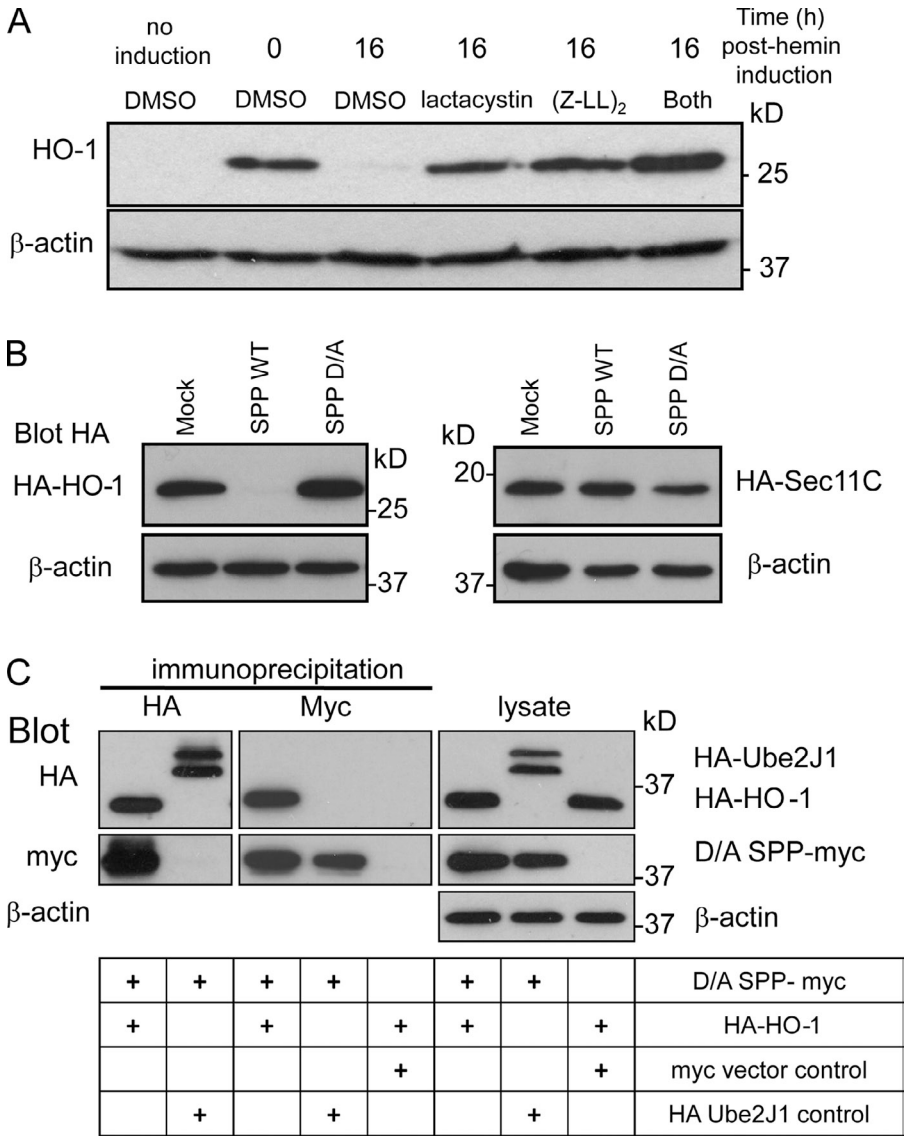

Figure 3. **Catalytically active SPP is required for HO-1 degradation.** (A) Immunoblot for HO-1. Endogenous HO-1 was induced with hemin (as in Fig. 2 C) in HEK-293T cells, and cells were harvested at indicated times, after incubation with control (DMSO), proteasome inhibitor (lactacystin), or SPP inhibitor ($(Z\text{-}LL)_2$ ketone). (B) HA immunoblot of overexpressed HA–HO-1 and HA-Sec11C cotransfected with GFP (mock), WT, or dominant-negative (D/A) SPP. (C) HA and myc immunoblots showing interaction between SPP (D/A) and HO-1. HEK-293T cells were cotransfected with empty myc vector or D265A SPP-myc KKEK (D/A SPP-myc) and either HA–HO-1 or HA-Ube2J1. NP-40/DOC lysates and eluates from the HA and myc immunoprecipitations were probed for the indicated proteins. Approximately 3% of the total cell lysates and ~25% of the immunoprecipitate eluates were loaded on the gels. Separate blots were exposed independently.

proteins, we tested the stability of four additional tail-anchored proteins: cytochrome B5A, the stress-inducible RAMP4 and RAMP4-2 (Yamaguchi et al., 1999), and Ube2J1. Like HO-1, cytochrome B5A RAMP4 and RAMP4-2 were rapidly degraded in the presence of WT SPP, in an SPP-dependent pathway, and were stabilized by D/A SPP (Fig. 5 A), whereas Ube2J1 was insensitive to SPP. To determine whether SPP affected degradation of endogenous protein, we induced RAMP4 with tunicamycin and, after removal of this stimulus, monitored the degradation of HO-1 in the presence or absence of SPP. As seen with endogenous HO-1, the degradation of RAMP4 was markedly reduced after siRNA-mediated SPP depletion in HeLa cells (Fig. 5 B). These data suggest that SPP-mediated cleavage and subsequent degradation are a feature of the degradation of many, but not all, ER-resident tail-anchored proteins.

Our results were extended with a series of chimeric proteins composed of the cytosolic and TMDs of HO-1, cytochrome B5A, or Ube2J1. All constructs containing the TMD of HO-1 and cytochrome B5A were degraded in an SPP-dependent pathway, whereas the TMD of Ube2J1 prevented SPP-dependent degradation (Fig. 5 C). The importance of the transmembrane region for cleavage by SPP was confirmed with two chimeric GFP proteins, with N-terminal GFP fused to either the TMD of SPP-sensitive HO-1 (GFP:HO-1TMD) or SPP-insensitive Ube2J1 (GFP:Ube2J1TMD). The HO-1 TMD construct was degraded in the presence of WT SPP and stabilized by mutant D/A SPP, $(Z\text{-}LL)_2$, and bortezomib (Fig. 5, D and E), whereas GFP:Ube2J1TMD remained SPP insensitive (Fig. 5 D). Collectively, these results suggest that cleavage by SPP, subsequent dislocation, and proteasome-mediated degradation are dependent on the transmembrane region.

SPP-mediated cleavage and dislocation are dependent on a minimal luminal domain

HO-1 has 266 predicted cytosolic N-terminal residues but only a very short luminal C-terminal tail (three to five residues). To determine how extension of the N-terminal cytosolic domain or C-terminal luminal domain affected HO-1 stability, we initially added a nine-residue HA tag to either the N or C terminus of HO-1 (HA–HO-1 and HO-1–HA, respectively). This short tag did not affect the rapid degradation or stabilization of HO-1 in cells expressing exogenous WT or D/A mutant SPP, respectively

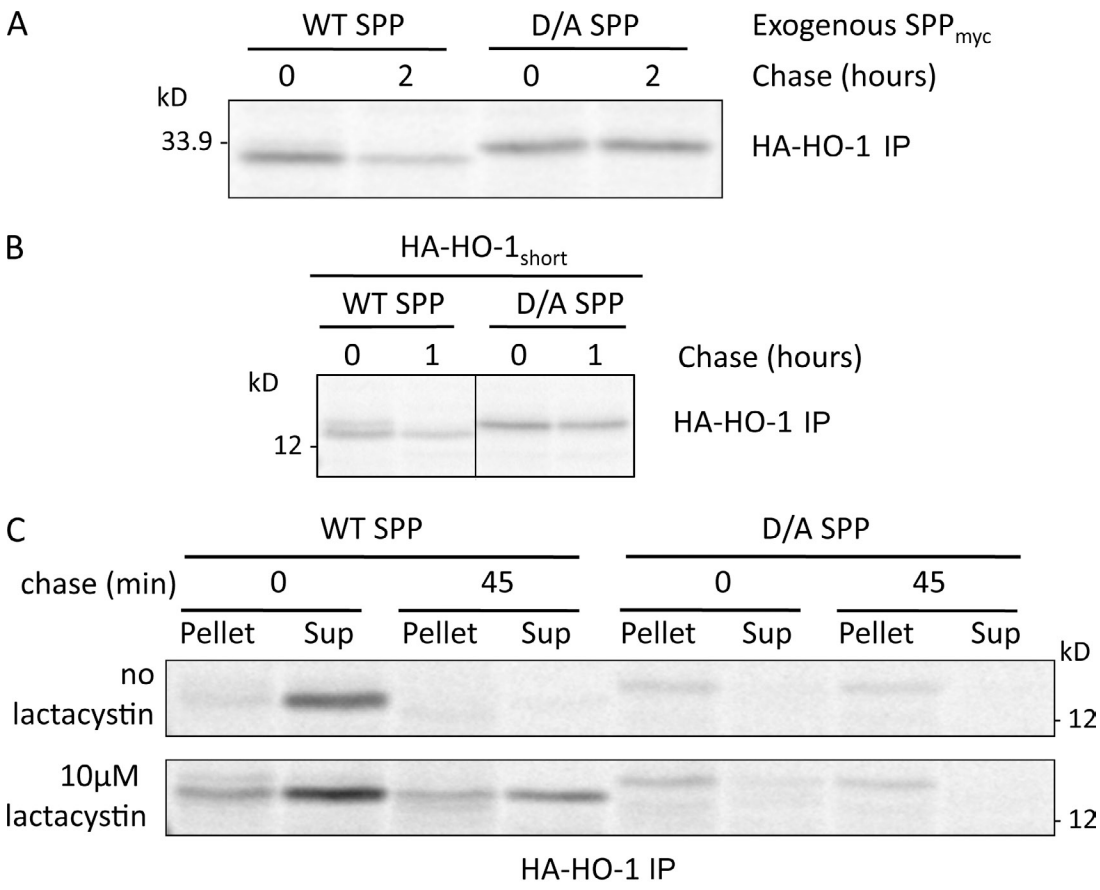

Figure 4. **HO-1 cleavage by catalytically active SPP is required for its dislocation from the ER membrane and subsequent proteasome-mediated degradation.** (A and B) Cleavage of HO-1 was visualized by metabolic label and pulse/chase analysis. Full-length HA–HO-1 (A) or truncated HO-1 (HA–HO-1_{short}; B) plasmids, together with either WT SPP or mutant (D/A) SPP plasmids were cotransfected into HEK-293T cells and [^{35}S]methionine/cysteine pulse labeled for 15 min. HO-1 was recovered by HA immunoprecipitation (IP) at the chase times indicated and analyzed by SDS-PAGE and autoradiography. The black line indicates that the middle lanes from gel were removed, so the second and third lanes were not contiguous. (C) HA–HO-1_{short} was transfected into HEK-293T cells together with either WT or mutant D/A SPP and radiolabeled as in B in the presence or absence of the proteasome inhibitor lactacystin. Postnuclear lysates were separated into membrane fractions (pellet) and soluble fractions (supernatant [Sup]) before HA immunoprecipitation, SDS-PAGE, and autoradiography.

(Fig. 6 A). We used this construct to confirm that the SPP-mediated cleavage of HO-1 occurs within the TMD, by comparing the expression of HA–HO-1 and HO-1–HA when coexpressed with WT SPP in the presence or absence of proteasome inhibitor. The HA–HO-1 protein is detected by both anti-HA and anti–HO-1 antibodies, when coexpressed with WT SPP, and detection is enhanced with bortezomib (Fig. S4, top). Upon transfer of the HA epitope from the N to the C terminus (HO-1–HA), both the noncleaved and cleaved form remain detectable with the HO-1 antibody, with the cleaved form protected by bortezomib. In contrast, HA now only detects the noncleaved form, and there is no rescue with bortezomib, as the small cleaved fragment is likely to be rapidly degraded (Fig. S4, bottom). Therefore, these experiments suggest that SPP-mediated cleavage of HO-1 occurs within the TMD.

Further luminal extension with the much larger GFP (238 residues; HO-1:GFP) prevented WT SPP-mediated degradation (Fig. 6 B, first through fourth lanes), whereas GFP fused to the cytosolic terminus (GFP:HO-1) was still rapidly degraded in the presence of WT SPP and stabilized by the SPP D/A mutant (Fig. 6 B, fifth through eighth lanes). To ensure that HO-1:GFP was inserted in the correct type II orientation, we confirmed that an N-linked glycosylation motif engineered into the GFP domain was both glycosylated and Endoglycosidase H sensitive (Fig. 6 B, first through fourth lanes), confirming its type II orientation in the ER membrane.

To further investigate the requirements for SPP-mediated cleavage, in particular how a bulky ER-luminal domain affects susceptibility to SPP-mediated cleavage and subsequent dislocation, we designed additional constructs, HA–HO-1.SP N/QIT and HA–HO-1.ΔSP N/QIT (von Heijne, 1986; Honsho et al., 1998). These HO-1 constructs have a luminal extension consisting of a T7 tag with an N-linked glycosylation motif (NIT) or control motif (QIT) and are otherwise identical except for five additional residues inserted between the membrane and the T7 tag of both constructs, which make HA–HO-1.SP N/QIT susceptible to cleavage by SP (Fig. 6 C, schematic), whereas the residues in HA–HO-1.ΔSP N/QIT are SP insensitive. Upon insertion into the ER membrane, both NIT-containing proteins were glycosylated, as determined by Endoglycosidase H sensitivity (Fig. 6 C, top). HA–HO-1.ΔSP NIT was relatively insensitive to SP and remained stable in the presence of WT SPP

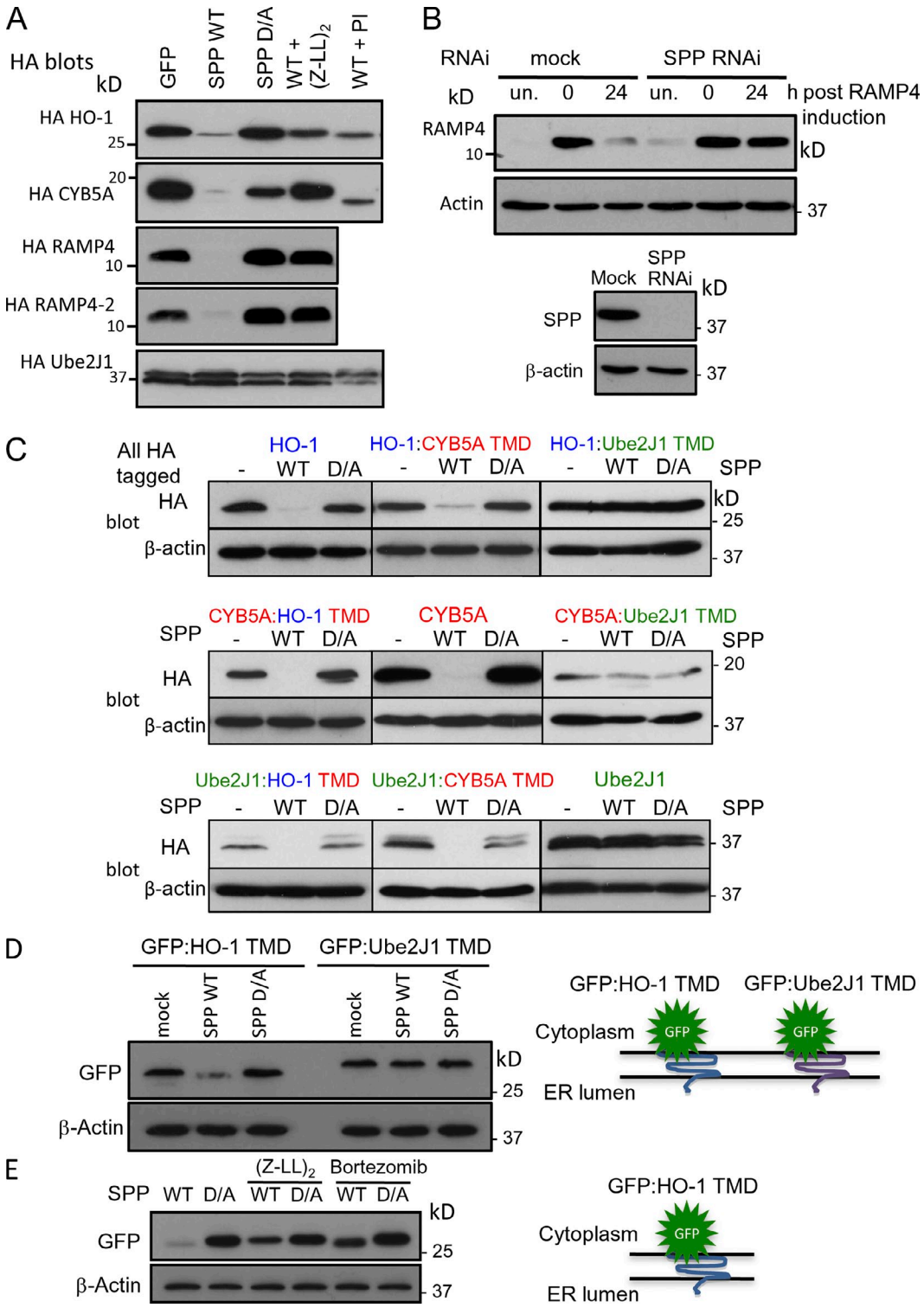

Figure 5. **ER-resident tail-anchored proteins are cleaved and degraded in an SPP-dependent pathway.** (A) HA immunoblot in HEK-293T cells cotransfected with either HA–HO-1, HA-CYB5A, HA-RAMP4, HA–RAMP4-2, or HA-Ube2J1 and either GFP (mock), WT, or dominant-negative (D/A) SPP as indicated. The SPP inhibitor $(Z\text{-}LL)_2$ ketone and the proteasome inhibitor lactacystin (PI) were added to the indicated samples 16 h before harvest. (B) Immunoblot for RAMP4. Mock- or SPP RNAi–transfected HeLa cells were treated with 1 µM tunicamycin for 17 h to induce RAMP4. Cells were harvested at 0 and 24 h after tunicamycin. Unstimulated cells (un.) were harvested at $t = 0$ h. The inset shows depletion of SPP at $t = 0$ h. (C) HA immunoblot in HEK-293T cells. Cotransfection with either WT or dominant-negative (D/A) SPP or GFP (−) and full-length or chimeric proteins as indicated. Chimeras contain the cytosolic domain of one protein fused to the transmembrane and luminal domain (TMD) as indicated by the color coding. Black lines indicate that intervening lanes have been spliced out. (D) Immunoblot for GFP in HEK-293T cells transfected with GFP fused to either the TMD of HO-1 (GFP:HO-1TMD) or the TMD of Ube2J1 (GFP:Ube2J1TMD) and either the empty vector (mock), WT, or dominant-negative (D/A) SPP as marked. (E) Immunoblot for GFP in HEK-293T cells transfected with GFP fused to the TMD of HO-1 (GFP:HO-1TMD) and either WT or dominant-negative (D/A) SPP. Samples were treated with the SPP inhibitor $(Z\text{-}LL)_2$ ketone or the proteasome inhibitor Bortezomib.

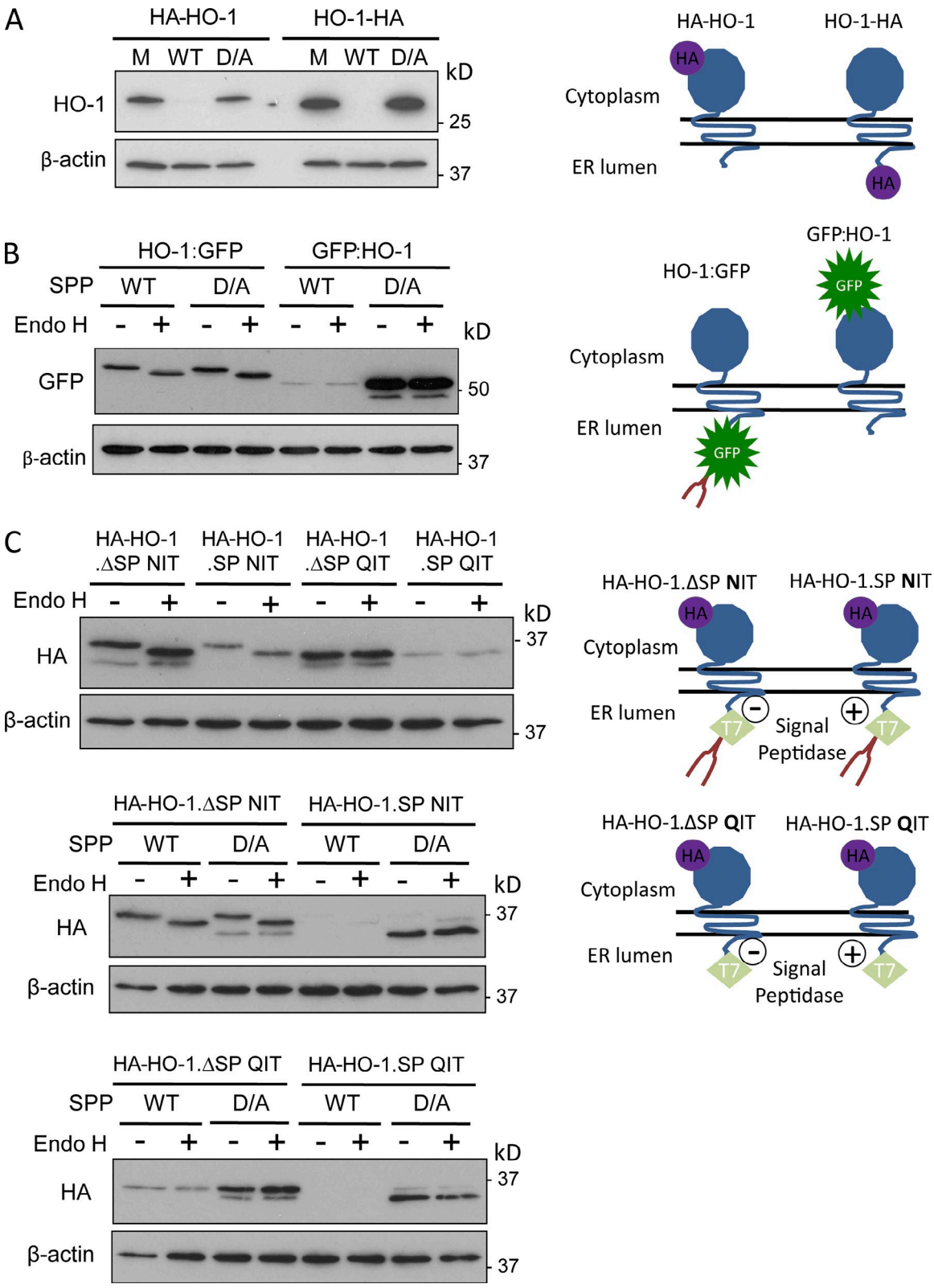

Figure 6. **The length of the luminal domain is a critical determinant of SPP-mediated cleavage.** (A) Immunoblot for HO-1 in HEK-293T cells cotransfected with either N-terminal (HA–HO-1) or C-terminal (HO-1–HA) HO-1 with or without WT, dominant-negative (D/A) SPP, or GFP (mock [M]) as indicated. (B) Immunoblot for GFP in HEK-293T cells transfected with either N-terminal (GFP:HO-1) or C-terminal (HO-1:GFP) GFP-tagged HO-1 with or without WT or dominant-negative (D/A) SPP. The GFP tag used in these constructs contained a double mutation (D82N and F84T; Grotzke et al., 2013) to generate an N-glycosylation site. Samples were subjected to Endoglycosidase H treatment (±Endo H). (C) Immunoblot for HA in HEK-293T cells transfected with HA–HO-1 constructs, which have an additional luminal tag, which starts with (SP) or without (ΔSP) a membrane proximal signal peptidase (SP) cleavage site, followed by a T7 tag and finishing with either a functional C-terminal N-glycosylation site (NIT) or a false N-glycosylation site (QIT) as shown in the schematic. These constructs were cotransfected with GFP (mock; top), WT, or (D/A) SPP and subjected to Endoglycosidase H treatment as indicated.

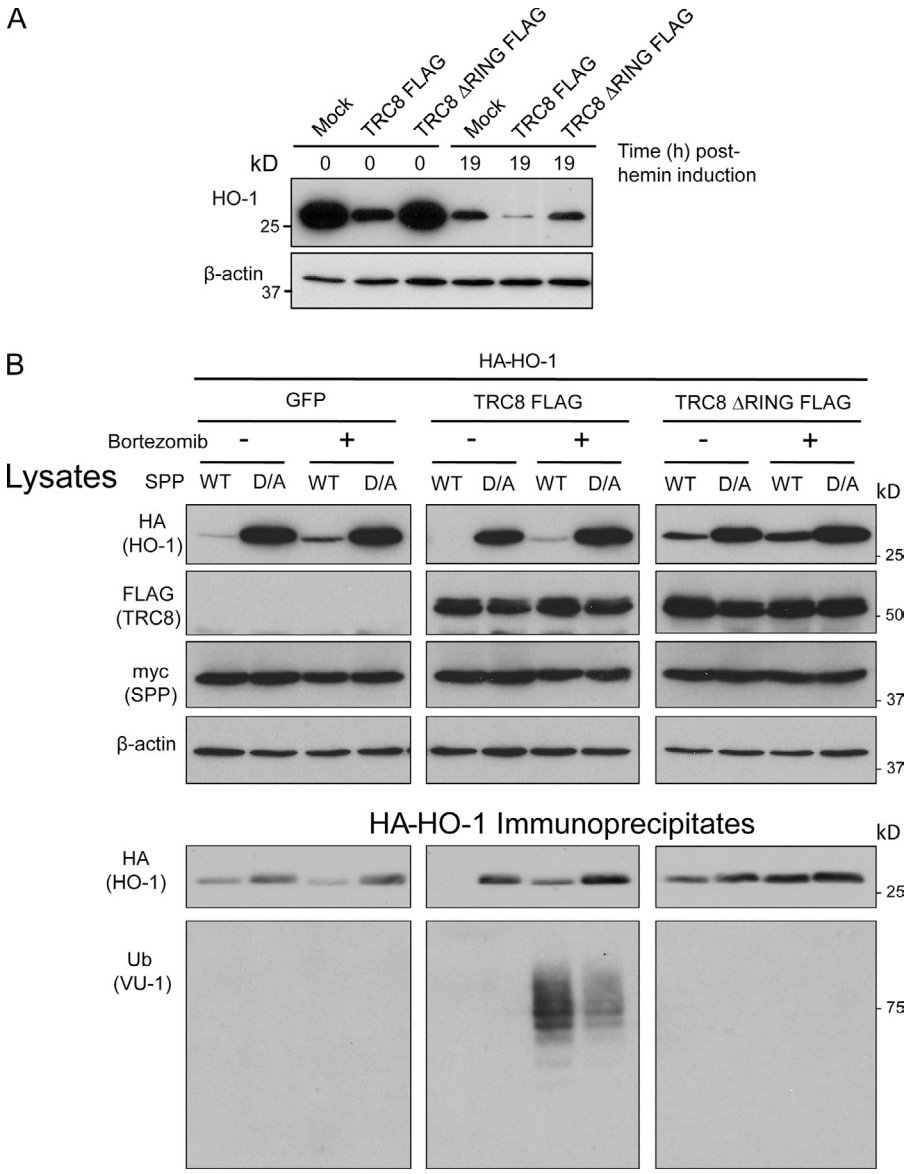

Figure 7. **TRC8 ubiquitinates cleaved HO-1.** (A) TRC8 expression decreases endogenous HO-1 levels. Immunoblot for HO-1. HEK-293T cells transfected with either GFP (mock), TRC8 FLAG, or TRC8 ΔRING FLAG were induced for 20 h with 50 µM hemin. Cells were harvested at the indicated times after hemin removal. (B) TRC8 ubiquitinates SPP-cleaved HO-1. HA, FLAG, myc, and ubiquitin immunoblots after cotransfection of HA–HO-1 with GFP (mock), TRC8 FLAG, TRC8 ΔRING FLAG, and either SPP myc KEKK (WT) or SPP myc KEKK D265A (D/A), in the presence (+) or absence (−) of Bortezomib. Lysates and HA (HA–HO-1) immunoprecipitations (performed under denaturing conditions) were probed for the indicated proteins.

(Fig. 6 C, middle, first through fourth lanes). In contrast, HA–HO-1.SP NIT was cleaved by SP and was rapidly degraded in the presence of WT SPP. When expressed with the SPP D/A mutant, HA–HO-1.SP NIT was stabilized in its SP cleaved, faster migrating form (Fig. 6 C, middle, fifth through eighth lanes). Both the nonglycosylated HA–HO-1.ΔSP QIT and HA–HO-1.SP QIT were degraded in the presence of WT SPP (Fig. 6 C, bottom, first, second, fifth, and sixth lanes) but stabilized by the SPP D/A mutant (Fig. 6 C, bottom, third, fourth, seventh, and eighth lanes).

These results show that cleavage by SPP and subsequent dislocation of HO-1 can be inhibited by either a bulky luminal extension (e.g., GFP) or an N-linked glycan. If the polypeptide is liberated, in the latter case by the cleavage of the ectodomain by SP, SPP-mediated cleavage proceeds, and the protein is degraded.

SPP cleavage triggers HO-1 ubiquitination by overexpressed TRC8

The association of TRC8 with SPP (Stagg et al., 2009) suggested a role for this E3 ligase in HO-1 ubiquitination and extraction from the ER membrane. Indeed, TRC8 was recently reported to be the E3 ligase responsible for the ubiquitination and degradation of HO-1 (Lin et al., 2013). This suggests that both ubiquitination and intramembrane cleavage are required for HO-1 dislocation. We find overexpressed TRC8 readily decreases induced endogenous HO-1 (Fig. 7 A), but in the cell lines tested, neither RNAi nor shRNA-mediated TRC8 depletion reproducibly protected HO-1 from degradation, suggesting the involvement of more than one E3 ligase or a redundancy in E3 ligase usage. With these caveats, we further examined the role of ubiquitination in HO-1 extraction, in particular to ascertain whether SPP cleavage enables HO-1 ubiquitination by overexpressed TRC8 or vice versa. Overexpressed HA–HO-1 was immunoprecipitated from bortezomib-treated cells that co-overexpress either control (GFP), TRC8, or the TRC8 ΔRING mutant (Stagg et al., 2009) with SPP WT or SPP D/A. Ubiquitinated HO-1 was readily detected after bortezomib treatment in TRC8/SPP but not TRC8 ΔRING/SPP– or GFP/SPP-treated cells. The ubiquitinated HO-1 species were more

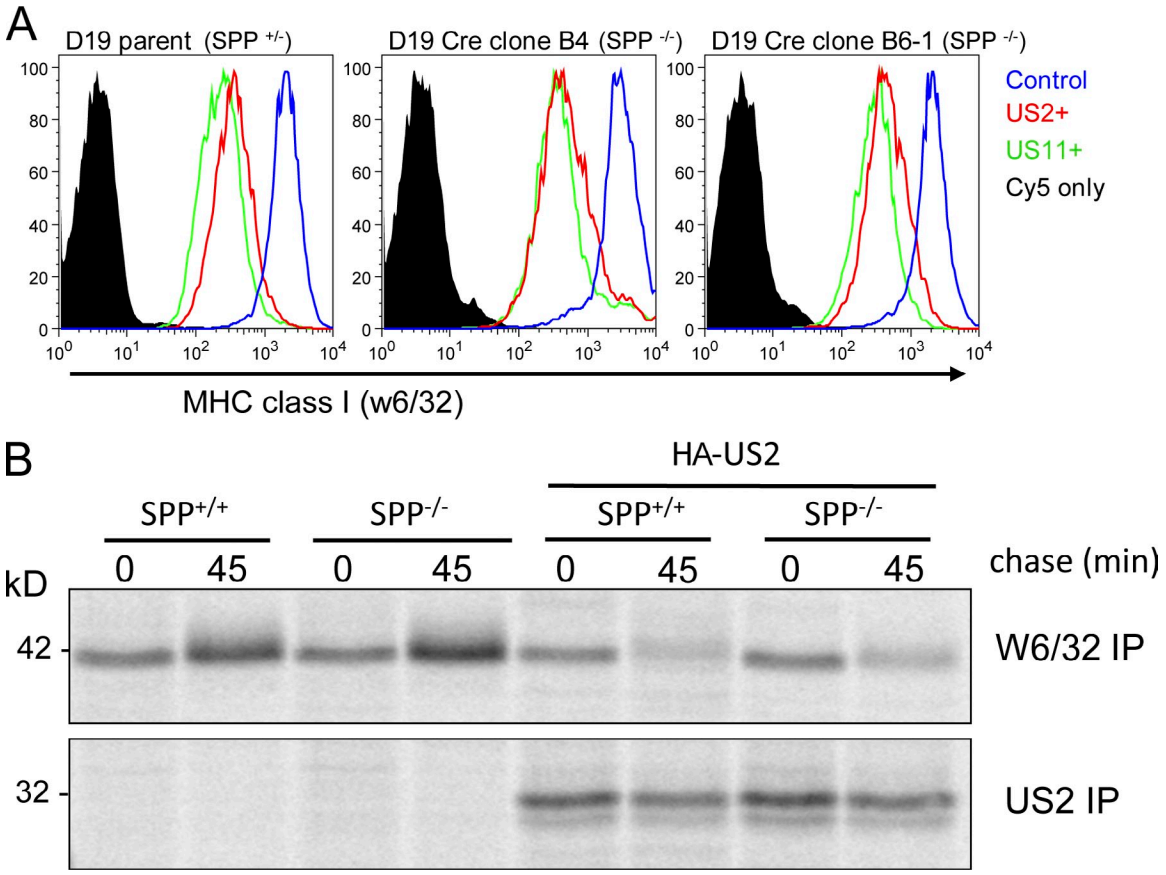

Figure 8. **SPP knockout HCT116 cells are competent for US2-mediated MHC class I dislocation.** (A) Cytofluorometric analysis of surface MHC class I expression (W6/32) in HCT116 clones transduced with mock lentivirus, US2-expressing lentivirus, or US11-expressing lentivirus. Solid black traces are cells stained with secondary antibody only (anti–mouse Alexa Fluor 647). (B) WT ($SPP^{+/+}$) and SPP knockout ($SPP^{-/-}$) HCT116 cells ± HA-US2 were pulse radiolabeled for 10 min, and MHC class I (W6/32) and US2 (rabbit anti-US2) were immunoprecipitated from detergent lysates at the times indicated. IP, immunoprecipitation.

prominent with SPP WT as compared with SPP D/A, despite much less HA–HO-1 being detected with SPP WT (Fig. 7 B). These experiments suggest that cleavage of HA–HO-1 is the primary event that precedes and may stimulate ubiquitination by TRC8, such that if cleavage does not occur, less HA–HO-1 ubiquitination is detected.

SPP is not required for the US2-mediated degradation of MHC-I molecules

SPP was previously implicated in the US2-mediated degradation of MHC-I (Loureiro et al., 2006), though no requirement for SPP's catalytic activity was reported. Despite successful RNAi- and shRNA-mediated depletions of SPP, we were unable to demonstrate a role for this protease in the US2-mediated degradation of MHC-I (Fig. S5). Because RNAi-mediated SPP depletion may not effectively abolish all enzymatic activity, we examined US2 function in the $SPP^{-/-}$ cells. Expression of US2 in the SPP knockout cells caused a decrease in cell surface MHC-I expression (Fig. 8 A), and pulse–chase analysis of [^{35}S]methionine/cysteine-radiolabeled cells showed rapid degradation of MHC-I with kinetics identical to SPP-replete WT parental cells (Fig. 8 B). Our results suggest that despite binding TRC8, SPP is not required for the US2-mediated degradation of MHC-I in these cells.

Discussion

Tail-anchored proteins represent 3–5% of all membrane proteins (Kalbfleisch et al., 2007). Here, we identify a novel function for SPP in the intramembrane cleavage and turnover of endogenous HO-1, an ER-resident tail-anchored protein. Our results suggest that SPP-mediated proteolysis is not limited to HO-1 but represents a more generalized pathway for turnover of additional members of this protein family.

The association of SPP with the TRC8 E3 ligase suggested a role for this intramembrane cleaving protease in ER protein turnover (Stagg et al., 2009), but we were unable to confirm a role for SPP in the US2-mediated degradation of MHC-I (Loureiro et al., 2006). However, the SPP somatic cell knockout enabled a functional proteomics screen, which identified HO-1 as a novel substrate of SPP, and emphasizes the utility of this unbiased approach. The predicted accumulation of membrane-embedded signal sequences from the ER membrane of SPP-deficient cells was not seen, probably a result of the difficulty of detecting short hydrophobic peptides by mass spectrometry. The twofold increase in the abundance of HO-1 in SPP knockout cells, though modest, likely reflects the very low resting level of constitutive HO-1 in nonstimulated cells. The ability to induce HO-1 expression, remove the stimulus, and monitor HO-1 degradation

over time provides a useful system to study the physiological turnover of an endogenous ER-resident protein.

Tail-anchored proteins represent an extreme example of type II transmembrane proteins with very short C termini in the ER lumen. The orientation of the catalytic sites in SPP's TMDs accounts for SPP's specificity for type II–oriented proteins (Weihofen et al., 2002). We did not identify type II proteins as SPP substrates, probably because the size of the luminal domain is critical in determining cleavage and subsequent degradation of HO-1 by SPP. Although Sec11c, a component of the SP complex, was our top hit by mass spectrometry from HCT116 cells, this could not be confirmed in HEK-293T cells, and we don't find Sec11c to be an SPP substrate.

The location of the hydrophobic transmembrane region very near the C terminus of HO-1 is characteristic for all tail-anchored proteins. Their insertion into the ER membrane is posttranslational and differs from cotranslational insertion in requiring TMD-selective cytosolic chaperones including the distinct GET (guided entry of tail-anchored proteins) pathway. (Shao and Hegde, 2011). Dislocation of tail-anchored proteins from the ER membrane may also be distinct from more conventional ERAD substrates. The absence of any substantive luminal domain in HO-1 means there is no clear requirement for luminal adaptors such as SEL1L to recognize luminal components. Nor is there necessarily a need to invoke a channel for the dislocation of tail-anchored proteins. Indeed, in the absence of any luminal domain, the main barrier to overcome is the energy required to dislocate the hydrophobic transmembrane region. In this regard, intramembrane cleavage of the TMD by SPP may be sufficient to destabilize the protein, reduce the energy barrier, and promote membrane extraction. Cleaved hydrophobic segments may also be less prone to aggregation once they are exposed to the cytosol.

Enzymatic cleavage by SPP and the related SPP-like proteases is classically viewed as a series of sequential proteolytic processing events (Voss et al., 2013). SPP's cleavage of tail-anchored proteins provides a unique example in which SPP's activity toward its substrate is the primary proteolytic event and does not require the sequential two-step proteolytic process, as seen after the cotranslational insertion of type I membrane protein with a signal sequence. Because tail-anchored proteins have no luminal domain, they require no initial processing, and cleavage by SPP is therefore the primary proteolytic event. SPP's activity may therefore have evolved for cleavage of tail-anchored proteins and was subsequently used for cleavage of other type II–orientated proteins after ectodomain removal.

Insertion of a small nine-residue luminal extension did not affect HO-1 stability, but the introduction of GFP or an N-linked glycan inhibited SPP cleavage and prevented degradation. This could be overcome by insertion of a SP recognition motif after the transmembrane region, with primary cleavage by SP liberating the HO-1 polypeptide for subsequent cleavage by SPP and degradation, presumably by allowing SPP access to the cleavage site. This is in keeping with the known activity of SPP after ectodomain shedding (Lemberg and Martoglio, 2002). SPP-mediated proteolysis may therefore enable dislocation of any protein with a type II orientation but, in such a case, would require an initiating proteolytic event to allow SPP to access its substrate. In the case of a single-pass type II transmembrane protein, this would simply involve removal of the luminal ectodomain. For a more complex polytopic protein, multiple proteolytic cleavage events might be required to expose a type II–orientated TMD to SPP-mediated cleavage. A role for SPP in ER quality control was originally suggested after the identification of SPP as a cross-linking partner of misfolded opsin (Crawshaw et al., 2004), and other membrane proteins associate with inactive SPP (Schrul et al., 2010).

HO-1 is rate limiting for the oxidative degradation of heme and is rapidly induced in conditions of oxidative stress, consistent with its critical in vitro and in vivo role as a cytoprotective enzyme (Poss and Tonegawa, 1997), through the antioxidative properties of biliverdin and carbon monoxide (Abraham and Kappas, 2008). Regulation of HO-1 expression is tightly controlled and occurs at the transcriptional (Yang and Zou, 2001), posttranscriptional (Leautaud and Demple, 2007), and posttranslational level (Lin et al., 2008). Our estimated half-life of HO-1 of 10 h is similar to that shown after treatment with cobalt protoporphyrin (Lin et al., 2008). Nitric oxide may be even more effective at increasing HO-1 concentration, through stabilization of HO-1 mRNA (Leautaud and Demple, 2007), consistent with the cytoprotective role of HO-1 in response to different forms of cellular stress. Although we do not see a stress-induced increase in SPP, as observed for other ERAD components, removal of the inducing signal leads to HO-1 degradation. Indeed, proteolysis provides an effective first step of enzyme inactivation, as soluble HO-1 has much reduced activity (Lin et al., 2007).

Therefore, in the simplest model for SPP-mediated HO-1 proteolysis, the rate of turnover of HO-1 by SPP does not change, but after the stimulation of HO-1 synthesis, its rate of production exceeds degradation, allowing HO-1 to accumulate in the ER membrane. After removal of this stimulus, the HO-1 is turned over by SPP until it returns to its resting equilibrium. In this regard, the half-life of other reported endogenous mammalian ERAD substrates is shorter than HO-1, varying from 30 to 90 min (Burr et al., 2011; Chen et al., 2011; Tyler et al., 2012), suggesting that SPP is involved in the turnover of this ER-resident protein and maintenance of ER homeostasis rather than regulation of misfolded proteins.

The degradation signal for SPP cleavage of HO-1 is likely imparted in the transmembrane region as transfer of this domain rendered an unrelated protein sensitive to SPP-mediated degradation. The length of the luminal extension is clearly critical, and UBE2J1, which is not an SPP substrate, has a longer luminal portion than the other tail-anchored proteins. However, engineered constructs with similar length luminal extensions were still cleaved by SPP. Although the TMD of HO-1 appears responsible for turnover, and is cleaved by SPP, it is unlikely to be disordered, as the transmembrane spans are in an α-helical conformation (Hwang et al., 2009). HO-1 oligomerization through its TMD is important for its catalytic activity. Degradation of HO-1 could therefore be triggered by loss of the oligomeric state, allowing access of SPP to the HO-1 monomer. However, a W270N HO-1 mutant, reported to interfere with oligomerization (Hwang et al., 2009), appeared less susceptible to SPP-mediated proteolysis (unpublished data). The formation of stable

transmembrane complexes might serve to sequester potential tail-anchored substrates away from SPP, with UBE2J1, for example, forming transmembrane associations with other ERAD components. This requires further examination, but our overexpression experiments should have overcome this possible effect. Helix-destabilizing residues in the membrane-spanning residues of signal peptides are reported to be important for intramembrane cleavage by SPP (Lemberg and Martoglio, 2002), and a larger range of tail-anchored proteins will need to be examined to determine whether this is also the case for these substrates.

The recent study of TRC8 as the E3 ligase responsible for the ubiquitination and degradation of HO-1 (Lin et al., 2013) fits well with our model of TRC8 binding SPP and suggests that both ubiquitination and intramembrane cleavage are required for HO-1 dislocation. Despite TRC8 overexpression readily decreasing HO-1 protein levels, neither RNAi- nor shRNA-mediated TRC8 depletion reproducibly protected HO-1 from degradation, suggesting that more than one E3 ligase may be involved or a redundancy in E3 ligase usage. Our TRC8 overexpression experiments indicate that SPP-mediated cleavage of HA–HO-1 precedes and may therefore trigger subsequent HO-1 ubiquitination by TRC8. Under these circumstances, cleavage by SPP will destabilize the protein and liberate a hydrophobic C-terminal peptide from the HO-1 TMD, which may in turn act as the degron for TRC8-mediated ubiquitination.

In summary, we have identified tail-anchored proteins as novel substrates of SPP and identified a crucial role for this enzyme in the intramembrane cleavage and subsequent degradation of HO-1 and other ER-resident tail-anchored proteins. A potential signaling role for HO-1 has been suggested, as a C-terminal truncated proteolytic fragment of HO-1 migrates to the nucleus to initiate a transcriptional program. Cleaved signal sequences such as the preprolactin signal peptide are also bioactive after their release from the ER membrane. Whether all the SPP-cleaved HO-1 is degraded by the proteasome or whether this pathway may act to initiate a transcriptional program for up-regulation of cytoprotective genes merits further study.

Materials and methods

Cell culture

HeLa cells were cultured in RPMI 1640 (PAA Laboratories). All other cells were cultured in Iscove's Modified Dulbecco's Media (PAA Laboratories) with 10% FBS (PAA Laboratories) and 100 U/ml penicillin and 100 µg/ml streptomycin (pen/strep; Sigma-Aldrich), in a humidified incubator with 5% CO_2 at 37°C. HO-1 was induced with 50 µM hemin (Sigma-Aldrich) in culture medium for 16–24 h, and degradation was induced by washing out the hemin once with PBS followed by incubation for 16–24 h in culture medium.

Antibodies

The following antibodies were used: rabbit anti-HA (PRB-101P; Covance), rabbit anti-SPP (ab16080; Abcam), rabbit anti–hepatitis C core (R4210; gift from J. McLauchlan, Medical Research Council–University of Glasgow Centre for Virus Research, Glasgow, Scotland, UK), mouse anti–HO-1 (ab13248; Abcam), mouse anti-myc (9B11; Cell Signaling Technology), mouse anti–β-actin (A5316; Sigma-Aldrich), rabbit anti-RAMP4/4-2 (A18; sc-85114; Santa Cruz Biotechnology, Inc.), mouse anti-calnexin (AF8) and rabbit anti-GFP (A11122; Invitrogen), rabbit anti-US2 (177–5; ER luminal domain; a gift from E. Wiertz, University Medical Center Utrecht, Utrecht, Netherlands), mouse anti–MHC-I (W6/32; ATCC), goat anti–mouse Alexa 647 (Invitrogen), goat anti–mouse IRDye 800 and goat anti–rabbit IRDye 680 (LI-COR Biosciences), and goat anti–mouse HRP and goat anti–rabbit HRP (Jackson ImmunoResearch Laboratories, Inc.).

Construction and isolation of HM13 (SPP) gene knockout

To construct the HM13 gene knockout, 5′ and 3′ arms of homology, flanking the HM13 exon 3, were generated by long-range PCR (LATaq; Takara Bio Inc.) from human genomic DNA, following the manufacturer's recommended conditions. To create the gene-targeting construct, the 5′ arm (5 kb) was introduced into the multicloning Spe1–Stu1 site of plasmid pOT7. Next, the 3′ arm (4.3 kb) was ligated (EcoR1–Not1) to generate pOT7:5:3. For the conditional targeting construct, HM13 exon 3 + LoxP was ligated directly upstream of the 3′ arm with Bgl2–EcoR1 to generate pOT7:5:E3M:3. Using two consecutive Gateway Cloning Technology reactions (Life Technologies), the promoterless mammalian positive selection cassette from plasmid pL1L2GT0-NEO (Skarnes et al., 2011) was inserted between the homology arms. This created the following plasmids: pOT7:5:3:SPPneo for permanent locus disruption and pOT7:5:E3M:3:conSPPneo for conditional gene targeting. For the first allele targeting, 30 µg plasmid pOT7:5:E3M:3:conSPPneo, linearized with Sal1, was electroporated into $\sim 1 \times 10^7$ HCT116 cells (0.55 kV, 25 µF, and 200 Ω; Gene Pulser; Bio-Rad Laboratories). After 48 h of incubation without selection, cells were split 1:10 into medium containing 1.8 mg/ml G418 (Life Technologies). After 2 wk of selection, genomic DNA was isolated from individual clones (Puregene Core Kit B; QIAGEN) and analyzed by long-range PCR to identify correct gene-targeting events. For further confirmation, HM13 mRNA, isolated from positive clones, was reverse transcribed into cDNA, amplified by PCR, and sequenced to confirm correct integration. To remove the targeting cassette and obtain the conditionally targeted allele, 2×10^6 clone 27 cells were electroporated (program D-32) with 2 µg pGFP_FLIP_IRES_PURO plasmid using Amaxa Kit V (Lonza). 2 d later, cells were selected with 1 µg/ml puromycin for 48 h (EMD Millipore) and seeded into 96-well plates at a cell density of 0.3 cells/well. Clones were replicate plated into either G418 or puromycin, and sensitive clones were confirmed for cassette loss by long-range PCR. This generated clone 27FLIP. The second allele of HM13 was targeted in clone 27FLIP for permanent disruption using linearized plasmid pOT7:5:3:SPPneo and the conditions described for the first allele targeting using plasmid pOT7:5:E3M:3:conSPPneo. Long-range PCR was used to identify G418-resistant clones that had lost exon 3 at the second allele.

To obtain fully SPP-deficient (−/−) cells, the LoxP-flanked exon 3 of HM13 was removed after lentiviral transduction with pHRSinGFP:Cre. GFP-positive clones were screened for Cre-mediated loss of HM13 exon 3 by long-range PCR. This resulted in clones B4 and B6-1.

Immunoblotting

Cells were either lysed directly using Laemmli loading buffer + Benzonase nuclease (Sigma-Aldrich) or using either 1% Triton X-100 or NP-40/DOC (1% NP-40 and 0.5% sodium deoxycholate) in TBS (10 mM Tris, pH 7.4, 150 mM NaCl, 1 mM $CaCl_2$, 1 mM $MgCl_2$, and 10 µM $ZnCl_2$) with protease inhibitors (1 mM iodoacetamide [Sigma-Aldrich], protease inhibitor cocktail [Roche], and 0.5 mM PMSF [Sigma-Aldrich]). Postnuclear lysates were then diluted into Laemmli buffer before SDS-PAGE (tris-tricine for core or tris-glycine for all other proteins). Samples were transferred to either nitrocellulose or polyvinylidene difluoride membranes, blocked, and incubated with primary and secondary antibodies as noted. Proteins were then visualized with chemiluminescent substrates (Thermo Fisher Scientific) or infrared imaging (Odyssey; LI-COR Biosciences). All blots were visualized by chemiluminescence unless otherwise indicated in the figure legend. For coimmunoprecipitation experiments, cells were lysed in NP-40/DOC in TBS plus protease inhibitors. Postnuclear lysates were precleared on IgG-Sepharose beads (GE Healthcare) and subjected to immunoprecipitation with EZview red anti-HA or anti–c-myc affinity gels (Sigma-Aldrich) as noted. Samples were washed with NP-40/DOC in TBS, dissociated from the beads by heating to 70°C for 5 min in reducing SDS sample buffer, and separated by SDS-PAGE and processed as described earlier for cell lysates. The HA–HO-1 ubiquitin immunoprecipitation experiment was performed as described for the coimmunoprecipitation experiments, except it was performed as a double HA immunoprecipitation, with elution from the first immunoprecipitation in 1% SDS in TBS and heating to 65°C for 5 min. The eluate was diluted to 0.1% SDS using NP-40/DOC in TBS buffer before the second immunoprecipitation and processed as described for the standard coimmunoprecipitation experiments.

Flow cytometry

Cells were stained with W6/32 monoclonal antibody (conformational MHC class I), followed by goat anti–mouse Alexa Fluor 647 (Invitrogen). Samples were processed on a FACSCalibur (BD) machine, and data were analyzed using FlowJo software (Tree Star).

Metabolic label and radioimmune precipitation

Radioimmune precipitation was performed as previously described (Burr et al., 2011). Cells were starved for 30 min in Met- and Cys-free medium and

labeled with [^{35}S]methionine/cysteine (NEN; PerkinElmer) for 10 min at 37°C. The label was chased with complete medium for the times indicated. Cells were washed in PBS and lysed in 1% NP-40 in TBS with protease inhibitors. Postnuclear lysates were cleared on IgG-Sepharose before immunoprecipitation with antibody plus protein A–Sepharose as indicated. After washing in 0.1% NP-40 in TBS, samples were dissociated from the beads and separated by SDS-PAGE. Radioactive proteins were visualized on a Storm scanner (GE Healthcare) and analyzed with ImageQuant TL software (GE Healthcare).

Mass spectrometry

WT (+/+) HCT116 and SPP knockout (−/−) clone B4 were grown in SILAC Iscove's Modified Dulbecco's Media (Thermo Fisher Scientific) supplemented with 10% dialyzed FBS, 500 µg/ml proline (to prevent arginine-proline interconversion), pen/strep, and either light (50 µg/ml Arg0 and Lys0) or heavy (50 µg/ml Arg10 and Lys8) amino acids, for nine generations to ensure 98% incorporation of the labeled amino acids. Cells were washed in PBS, harvested by scraping, and resuspended in hypotonic lysis buffer (50 mM Tris-HCl, pH 7.4, 1 mM $MgCl_2$, 1 mM $CaCl_2$, 10 µM $ZnCl_2$, and protease inhibitors). Cells were lysed by three serial freeze/thaw cycles before nuclei, and unlysed cells were removed by a 5,000 *g* spin. The nonnuclear membranes were then pelleted at 100,000 *g* for 1.5 h and washed with 1 M sodium carbonate, and the pellets were resuspended in 8 M urea. 250 µg protein was digested using the filter-aided sample preparation protocol, and the resulting tryptic peptides were fractionated using high-pH reversed-phase HPLC. A total of 53 fractions were analyzed using a mass spectrometer (Orbitrap XL; Thermo Fisher Scientific) coupled to a nanoAcquity HPLC (Waters). Peptides were resolved using a 25-cm ethylene bridged hybrid column with a gradient rising from 3 to 25% MeCN over 30 min, 45% MeCN by 45 min, and 85% MeCN by 50 min. Eluting peptides were subjected to mass spectrometry between a 300 and 2,000 mass per charge at 60,000 full width at half-maximum resolution. Peptides were selected for collision-induced dissociation fragmentation using a Top6 data-dependent acquisition with fragmented peptides excluded for 3 min.

Data were processed using MaxQuant v.1.3.0.5 against the UniProt Human database (downloaded October 16, 2013). Carbamidomethyl (C) was defined as a fixed modification with acetylation (protein N terminus), and deamidation (NQ) and oxidation (M) were defined as potential variable modifications. Requant was turned on, and a minimum ratio count of 1 was required for quantitation, but reported proteins needed to be quantified in both the forward and reverse experiment. Postprocessing data manipulation was performed in Perseus v.1.4.0.0.

RNA sequence analysis

Total RNA was harvested from three biological replicates of nonconfluent HCT116 ($SPP^{+/+}$) and B4 ($SPP^{-/-}$) cells (RNeasy kit; QIAGEN). RNA integrity was verified on a 2100 Bioanalyzer (Agilent Technologies) before preparing cDNA libraries using a RNA kit (TruSeq; Illumina). Libraries were sequenced on a HiSeq platform (Illumina). Reads were aligned to the human genome using CLC Genomics Workbench (QIAGEN), and RNA-Seq analysis of the mapped reads was performed using Avadis NGS (Strand Scientific). Differentially expressed genes were identified by the fold change method using a Benjamin–Hochberg's false discovery rate of $P < 1 \times 10^{-4}$.

Plasmid constructs

The lentiviral expression plasmids are based on a pHR vector obtained from A. Thrasher (Center for Immunodeficiency, Institute of Child Health, University College London, London, England, UK; Demaison et al., 2002) and were gifts from Y. Ikeda (Mayo Clinic, Rochester, MN). A plasmid expressing the envelope protein from vesicular stomatitis virus (pMD-G) and the lentiviral packaging plasmid pCMVR8.91 were used in conjunction with the lentiviral expression plasmids to produce self-inactivating lentiviral particles for transduction. The SPP-expressing lentiviral plasmids pHRSIN SPPwt myc KKEK (WT SPP) and pHRSIN SPP D256A myc KKEK (D/A SPP) were subcloned from plasmids pRK SPPwt myc KKEK and pRK SPP D265A myc KKEK (gifts from B. Dobberstein, German Cancer Research Center and the Center for Molecular Biology of the University of Heidelberg Alliance, Heidelberg, Germany; Schrul et al., 2010). The core-expressing lentiviral plasmids pHRSIN CMVp core-WT and pHRSIN CMVp core-F130E express hepatitis C virus core plus part of E1 and were subcloned from the RNA expression plasmids pSFV1 core-E1E2 and pSFV1 core-F130E (gifts from J. McLauchlan; Boulant et al., 2006). HA-US2 and HA-US11 were subcloned into a lentiviral vector that coexpresses the puromycin (puro) resistance gene (pHRSINpgkPURO). pHRSIN HA–HO-1 puro (HA–HO-1) and pHRSIN HO-1–HA puro (HO-1–HA) were generated by subcloning WT HO-1 from Flag3-full-length HO-1 (a gift of L.-Y. Chau, Institute of Biomedical Sciences, Academia Sinica, Taipei, Taiwan), into pHRSIN HA (N terminus) pgkPURO and pHRSIN HA (C terminus) pgkPURO lentiviral expression plasmids (HO-1–HA C-terminal tag sequence is AAAYPYDVPDYA*; The asterisk represents termination via a STOP codon.). pHRSIN HA–$HO\text{-}1_{short}$ puro (HA–$HO\text{-}1_{short}$) contains a 154–amino acid deletion (Δ30–184) engineered by site-directed deletion of nucleotides 91–552 of the HO-1 coding sequence cloned into pHRSIN HA (N terminus) pgkPURO. pHRSIN HA-Sec11c puro (HA-Sec11c) was generated by PCR amplification from pCMV6-XL5 Secllc (OriGene) and cloned into pHRSIN HA (N terminus) pgkPURO. pHRSIN HA-Ube2J1 puro (HA-Ube2J1) was generated by PCR amplification from IMAGE clone 4137664 and cloned into pHRSIN HA (N terminus) pgkPURO. pHRSIN HA CYB5A puro (HA-CYB5A), pHRSIN HA RAMP4 puro (HA-RAMP4), and pHRSIN HA RAMP4-2 puro (HA–RAMP4-2) were generated by PCR amplification from a human fetal brain yeast two-hybrid cDNA library (Invitrogen) and cloned into pHRSIN HA (N terminus) pgkPURO. pHRSIN $EmGFP^{glyc}$:HO-1 (GFP:HO-1) and pHRSIN HO-1.$EmGFP^{glyc}$ (HO-1:GFP) were generated by subcloning WT HO-1 into pHRSIN $EmGFP^{glyc}$ (N terminus) and pHRSIN $EmGFP^{glyc}$ (C terminus) lentiviral expression plasmids. $EmGFP^{glyc}$ is modified to include a glycosylation site by the introduction of D82N and F84T changes, as previously described (Grotzke et al., 2013). pHRSIN HA–HO-1:SP:T7:Glyc puro (HA–HO-1.SP NIT), pHRSIN HA–HO-1:ΔSP:T7:Glyc puro (HA–HO-1.ΔSP NIT), pHRSIN HA–HO-1:SP:T7:ΔGlyc puro (HA–HO-1.SP QIT), and pHRSIN HA–HO-1:ΔSP:T7:ΔGlyc puro (HA–HO-1.ΔSP QIT) were generated by cloning the full-length heme oxygenase coding sequence (minus the stop codon) along with an oligonucleotide pair encoding either a short SP cleavage or ΔSP cleavage-modifying sequence, a T7 tag (MASMTGGQQMG), and a glycosylation (NIT) or false glycosylation (QIT) sequence into pHRSIN HA (N terminus) pgkPURO. The short SP cleavage-modifying sequence in HA–HO-1.SP constructs demonstrated enhanced cleavage by SP compared with the sequence encoded in HA–HO-1.ΔSP constructs. The translated C-terminal tag sequences are HA–HO-1.SP NIT translation, PLPQPMASMTGGQQMGNITQPSPA*; HA–HO-1.ΔSP NIT translation, ALAQPMASMTGGQQMGNITQPSPA*; HA–HO-1.SP QIT translation, PLPQPMASMTGGQQMGQITQPSPA*; and HA–HO-1.ΔSP QIT translation, ALAQPMASMTGGQQMGQITQPSPA*. pHRSIN GFP:HO-1 TMD (GFP:HO-1TMD) and pHRSIN GFP:Ube2J1 TMD (GFP:Ube2J1TMD) were generated by subcloning the coding sequence for the C-terminal 26 amino acids of HO-1 or for the C-terminal 42 amino acids of Ube2J1 into a pHRSIN GFP (N terminus) lentiviral expression plasmid. The cytoplasmic domain:transmembrane and luminal domain (TMD) fusion proteins examined in Fig. 5 C were generated by pairing the cytoplasmic domain from one tail-anchored protein with the transmembrane and luminal domain of another tail-anchored protein, as shown. This was achieved by combining the coding sequence (BamHI–SpeI compatible ends) for each cytoplasmic domain (HO-1 amino acids 1–261, CYB5A amino acids 1–106, and Ube2J1 amino acids 1–281) with the coding sequence (SpeI–NotI compatible ends, including a stop codon) for the required transmembrane and luminal domain (TMD) (HO-1 amino acids 263–288, CYB5A amino acids 108–134, and Ube2J1 amino acids 282–318). These were ligated as pairs, into pHRSIN HA (N terminus) pgkPURO (BamHI–NotI) to give the required HA-tagged chimeric constructs.

Transient transfection, lentiviral transduction, and RNAi knockdown

HCT116 cells were transfected with jetPRIME (Polyplus Transfection), whereas HEK-293T cells were transfected with 293 TransIT (Mirus Bio LLC). Lentiviral expression and packaging plasmids were cotransfected into HEK-293T cells to produce lentiviral particles encoding HA-US2, HA-US11, Cre recombinase, GFP, hepatitis C virus core F130E, SPPwt myc KKEK, or SPP D/A myc KKEK. These particles were used to transduce cells, and when appropriate, stable clones were isolated after selection with puromycin (EMD Millipore). RNAi knockdown of SPP in HeLa cells was performed using an ON-TARGETplus siRNA pool against human HM13 (Thermo Fisher Scientific) transfected using Oligofectamine (Invitrogen).

Online supplemental material

Fig. S1 shows a schematic representation of the design and strategy used to generate a somatic cell knockout of HM13. Fig. S2 shows PCR confirmation of the intermediate and completed HM13 knockout cells. Fig. S3 shows alternate splicing of HM13 mRNA transcripts in the $SPP^{+/+}$ parental HCT116 cell line and the $SPP^{-/-}$ cell line D19CreB4. Fig. S4 shows that SPP-mediated cleavage of HO-1 occurs within its C-terminal TMD, as shown by the absence of the faster migrating HO-1–HA band when detected with an HA antibody compared with detection with an HO-1 antibody. Fig. S5 shows that siRNA-mediated knockdown of SPP does not rescue US2-mediated downregulation of MHC-I. Table S1 lists the plasmids used in the production of the

HM13 knockout cell line D19CreB4. Table S2 contains a brief description and the nucleotide sequence of the primers used to confirm and produce the HM13 knockout cell line D19CreB4. Table S3 shows confirmatory sequence analysis of mRNA from the first allele knockout cells described in Fig. S2 B. Table S4 contains RNA-Seq analysis of the $SPP^{-/-}$ cell line D19CreB4 versus the $SPP^{+/+}$ parental HCT116 cell line. Online supplemental material is available at http://www.jcb.org/cgi/content/full/jcb.201312009/DC1.

We thank Manu Hegde, John Mclauchlan, and the Lehner laboratory for helpful discussions and Abdul Sesay and the National Institute for Medical Research Sequencing facility for help with RNA-Seq analysis.

This work was supported by a Wellcome Trust Principal Research Fellowship to P.J. Lehner, Medical Research Council grant numbers U105170648 to F. Randow and U117597140 to J.C. Smith, and by the National Institute for Health Research Cambridge Biomedical Research Centre. The Cambridge Institute for Medical Research is in receipt of a Wellcome Trust Strategic Award.

The authors declare no competing financial interests.

Submitted: 2 December 2013
Accepted: 19 May 2014

References

Abraham, N.G., and A. Kappas. 2008. Pharmacological and clinical aspects of heme oxygenase. *Pharmacol. Rev.* 60:79–127. http://dx.doi.org/10.1124/pr.107.07104

Blom, D., C. Hirsch, P. Stern, D. Tortorella, and H.L. Ploegh. 2004. A glycosylated type I membrane protein becomes cytosolic when peptide: N-glycanase is compromised. *EMBO J.* 23:650–658. http://dx.doi.org/10.1038/sj.emboj.7600090

Boulant, S., R. Montserret, R.G. Hope, M. Ratinier, P. Targett-Adams, J.P. Lavergne, F. Penin, and J. McLauchlan. 2006. Structural determinants that target the hepatitis C virus core protein to lipid droplets. *J. Biol. Chem.* 281:22236–22247. http://dx.doi.org/10.1074/jbc.M601031200

Brodsky, J.L. 2012. Cleaning up: ER-associated degradation to the rescue. *Cell*. 151:1163–1167. http://dx.doi.org/10.1016/j.cell.2012.11.012

Burr, M.L., F. Cano, S. Svobodova, L.H. Boyle, J.M. Boname, and P.J. Lehner. 2011. HRD1 and UBE2J1 target misfolded MHC class I heavy chains for endoplasmic reticulum-associated degradation. *Proc. Natl. Acad. Sci. USA*. 108:2034–2039. http://dx.doi.org/10.1073/pnas.1016229108

Carvalho, P., V. Goder, and T.A. Rapoport. 2006. Distinct ubiquitin-ligase complexes define convergent pathways for the degradation of ER proteins. *Cell*. 126:361–373. http://dx.doi.org/10.1016/j.cell.2006.05.043

Chen, X., H. Tukachinsky, C.H. Huang, C. Jao, Y.R. Chu, H.Y. Tang, B. Mueller, S. Schulman, T.A. Rapoport, and A. Salic. 2011. Processing and turnover of the Hedgehog protein in the endoplasmic reticulum. *J. Cell Biol.* 192:825–838. http://dx.doi.org/10.1083/jcb.201008090

Christianson, J.C., J.A. Olzmann, T.A. Shaler, M.E. Sowa, E.J. Bennett, C.M. Richter, R.E. Tyler, E.J. Greenblatt, J.W. Harper, and R.R. Kopito. 2012. Defining human ERAD networks through an integrative mapping strategy. *Nat. Cell Biol.* 14:93–105. http://dx.doi.org/10.1038/ncb2383

Crawshaw, S.G., B. Martoglio, S.L. Meacock, and S. High. 2004. A misassembled transmembrane domain of a polytopic protein associates with signal peptide peptidase. *Biochem. J.* 384:9–17. http://dx.doi.org/10.1042/BJ20041216

Demaison, C., K. Parsley, G. Brouns, M. Scherr, K. Battmer, C. Kinnon, M. Grez, and A.J. Thrasher. 2002. High-level transduction and gene expression in hematopoietic repopulating cells using a human immunodeficiency [correction of imunodeficiency] virus type 1-based lentiviral vector containing an internal spleen focus forming virus promoter. *Hum. Gene Ther.* 13:803–813. http://dx.doi.org/10.1089/10430340252898984

Fleig, L., N. Bergbold, P. Sahasrabudhe, B. Geiger, L. Kaltak, and M.K. Lemberg. 2012. Ubiquitin-dependent intramembrane rhomboid protease promotes ERAD of membrane proteins. *Mol. Cell*. 47:558–569. http://dx.doi.org/10.1016/j.molcel.2012.06.008

Golde, T.E., M.S. Wolfe, and D.C. Greenbaum. 2009. Signal peptide peptidases: a family of intramembrane-cleaving proteases that cleave type 2 transmembrane proteins. *Semin. Cell Dev. Biol.* 20:225–230. http://dx.doi.org/10.1016/j.semcdb.2009.02.003

Greenblatt, E.J., J.A. Olzmann, and R.R. Kopito. 2011. Derlin-1 is a rhomboid pseudoprotease required for the dislocation of mutant α-1 antitrypsin from the endoplasmic reticulum. *Nat. Struct. Mol. Biol.* 18:1147–1152. http://dx.doi.org/10.1038/nsmb.2111

Greenblatt, E.J., J.A. Olzmann, and R.R. Kopito. 2012. Making the cut: intramembrane cleavage by a rhomboid protease promotes ERAD. *Nat. Struct. Mol. Biol.* 19:979–981. http://dx.doi.org/10.1038/nsmb.2398

Grotzke, J.E., Q. Lu, and P. Cresswell. 2013. Deglycosylation-dependent fluorescent proteins provide unique tools for the study of ER-associated degradation. *Proc. Natl. Acad. Sci. USA*. 110:3393–3398. http://dx.doi.org/10.1073/pnas.1300328110

Hegde, R.S., and H.L. Ploegh. 2010. Quality and quantity control at the endoplasmic reticulum. *Curr. Opin. Cell Biol.* 22:437–446. http://dx.doi.org/10.1016/j.ceb.2010.05.005

Honsho, M., J.Y. Mitoma, and A. Ito. 1998. Retention of cytochrome b5 in the endoplasmic reticulum is transmembrane and luminal domain-dependent. *J. Biol. Chem.* 273:20860–20866. http://dx.doi.org/10.1074/jbc.273.33.20860

Huppa, J.B., and H.L. Ploegh. 1997. The alpha chain of the T cell antigen receptor is degraded in the cytosol. *Immunity*. 7:113–122. http://dx.doi.org/10.1016/S1074-7613(00)80514-2

Hwang, H.W., J.R. Lee, K.Y. Chou, C.S. Suen, M.J. Hwang, C. Chen, R.C. Shieh, and L.Y. Chau. 2009. Oligomerization is crucial for the stability and function of heme oxygenase-1 in the endoplasmic reticulum. *J. Biol. Chem.* 284:22672–22679. http://dx.doi.org/10.1074/jbc.M109.028001

Kalbfleisch, T., A. Cambon, and B.W. Wattenberg. 2007. A bioinformatics approach to identifying tail-anchored proteins in the human genome. *Traffic*. 8:1687–1694. http://dx.doi.org/10.1111/j.1600-0854.2007.00661.x

Kostova, Z., Y.C. Tsai, and A.M. Weissman. 2007. Ubiquitin ligases, critical mediators of endoplasmic reticulum-associated degradation. *Semin. Cell Dev. Biol.* 18:770–779. http://dx.doi.org/10.1016/j.semcdb.2007.09.002

Leautaud, V., and B. Demple. 2007. Regulation of heme oxygenase-1 mRNA deadenylation and turnover in NIH3T3 cells by nitrosative or alkylation stress. *BMC Mol. Biol.* 8:116. http://dx.doi.org/10.1186/1471-2199-8-116

Lemberg, M.K., and B. Martoglio. 2002. Requirements for signal peptide peptidase-catalyzed intramembrane proteolysis. *Mol. Cell*. 10:735–744. http://dx.doi.org/10.1016/S1097-2765(02)00655-X

Lemberg, M.K., and B. Martoglio. 2004. On the mechanism of SPP-catalysed intramembrane proteolysis; conformational control of peptide bond hydrolysis in the plane of the membrane. *FEBS Lett.* 564:213–218. http://dx.doi.org/10.1016/S0014-5793(04)00192-9

Li, W., M.H. Bengtson, A. Ulbrich, A. Matsuda, V.A. Reddy, A. Orth, S.K. Chanda, S. Batalov, and C.A. Joazeiro. 2008. Genome-wide and functional annotation of human E3 ubiquitin ligases identifies MULAN, a mitochondrial E3 that regulates the organelle's dynamics and signaling. *PLoS ONE*. 3:e1487. http://dx.doi.org/10.1371/journal.pone.0001487

Lilley, B.N., and H.L. Ploegh. 2005. Viral modulation of antigen presentation: manipulation of cellular targets in the ER and beyond. *Immunol. Rev.* 207:126–144. http://dx.doi.org/10.1111/j.0105-2896.2005.00318.x

Lin, P.H., M.T. Chiang, and L.Y. Chau. 2008. Ubiquitin-proteasome system mediates heme oxygenase-1 degradation through endoplasmic reticulum-associated degradation pathway. *Biochim. Biophys. Acta*. 1783:1826–1834. http://dx.doi.org/10.1016/j.bbamcr.2008.05.008

Lin, P.H., W.M. Lan, and L.Y. Chau. 2013. TRC8 suppresses tumorigenesis through targeting heme oxygenase-1 for ubiquitination and degradation. *Oncogene*. 32:2325–2334. http://dx.doi.org/10.1038/onc.2012.244

Lin, Q., S. Weis, G. Yang, Y.H. Weng, R. Helston, K. Rish, A. Smith, J. Bordner, T. Polte, F. Gaunitz, and P.A. Dennery. 2007. Heme oxygenase-1 protein localizes to the nucleus and activates transcription factors important in oxidative stress. *J. Biol. Chem.* 282:20621–20633. http://dx.doi.org/10.1074/jbc.M607954200

Loo, T.W., and D.M. Clarke. 1998. Quality control by proteases in the endoplasmic reticulum. Removal of a protease-sensitive site enhances expression of human P-glycoprotein. *J. Biol. Chem.* 273:32373–32376. http://dx.doi.org/10.1074/jbc.273.49.32373

Loureiro, J., B.N. Lilley, E. Spooner, V. Noriega, D. Tortorella, and H.L. Ploegh. 2006. Signal peptide peptidase is required for dislocation from the endoplasmic reticulum. *Nature*. 441:894–897. http://dx.doi.org/10.1038/nature04830

Mann, M. 2006. Functional and quantitative proteomics using SILAC. *Nat. Rev. Mol. Cell Biol.* 7:952–958. http://dx.doi.org/10.1038/nrm2067

McLauchlan, J. 2009. Lipid droplets and hepatitis C virus infection. *Biochim. Biophys. Acta*. 1791:552–559. http://dx.doi.org/10.1016/j.bbalip.2008.12.012

McLauchlan, J., M.K. Lemberg, G. Hope, and B. Martoglio. 2002. Intramembrane proteolysis promotes trafficking of hepatitis C virus core protein to lipid droplets. *EMBO J.* 21:3980–3988. http://dx.doi.org/10.1093/emboj/cdf414

Mehnert, M., T. Sommer, and E. Jarosch. 2010. ERAD ubiquitin ligases: multifunctional tools for protein quality control and waste disposal in the endoplasmic reticulum. *Bioessays*. 32:905–913. http://dx.doi.org/10.1002/bies.201000046

Poss, K.D., and S. Tonegawa. 1997. Reduced stress defense in heme oxygenase 1-deficient cells. *Proc. Natl. Acad. Sci. USA*. 94:10925–10930. http://dx.doi.org/10.1073/pnas.94.20.10925

Ryter, S.W., J. Alam, and A.M. Choi. 2006. Heme oxygenase-1/carbon monoxide: from basic science to therapeutic applications. *Physiol. Rev.* 86:583–650. http://dx.doi.org/10.1152/physrev.00011.2005

Schneider, C.A., W.S. Rasband, and K.W. Eliceiri. 2012. NIH Image to ImageJ: 25 years of image analysis. *Nat. Methods*. 9:671–675. http://dx.doi.org/10.1038/nmeth.2089

Schrul, B., K. Kapp, I. Sinning, and B. Dobberstein. 2010. Signal peptide peptidase (SPP) assembles with substrates and misfolded membrane proteins into distinct oligomeric complexes. *Biochem. J.* 427:523–534. http://dx.doi.org/10.1042/BJ20091005

Shao, S., and R.S. Hegde. 2011. Membrane protein insertion at the endoplasmic reticulum. *Annu. Rev. Cell Dev. Biol.* 27:25–56. http://dx.doi.org/10.1146/annurev-cellbio-092910-154125

Skarnes, W.C., B. Rosen, A.P. West, M. Koutsourakis, W. Bushell, V. Iyer, A.O. Mujica, M. Thomas, J. Harrow, T. Cox, et al. 2011. A conditional knockout resource for the genome-wide study of mouse gene function. *Nature*. 474:337–342. http://dx.doi.org/10.1038/nature10163

Stagg, H.R., M. Thomas, D. van den Boomen, E.J. Wiertz, H.A. Drabkin, R.M. Gemmill, and P.J. Lehner. 2009. The TRC8 E3 ligase ubiquitinates MHC class I molecules before dislocation from the ER. *J. Cell Biol.* 186:685–692. http://dx.doi.org/10.1083/jcb.200906110

Tyler, R.E., M.M. Pearce, T.A. Shaler, J.A. Olzmann, E.J. Greenblatt, and R.R. Kopito. 2012. Unassembled CD147 is an endogenous endoplasmic reticulum-associated degradation substrate. *Mol. Biol. Cell*. 23:4668–4678. http://dx.doi.org/10.1091/mbc.E12-06-0428

Vashist, S., and D.T. Ng. 2004. Misfolded proteins are sorted by a sequential checkpoint mechanism of ER quality control. *J. Cell Biol.* 165:41–52. http://dx.doi.org/10.1083/jcb.200309132

von Heijne, G. 1986. A new method for predicting signal sequence cleavage sites. *Nucleic Acids Res.* 14:4683–4690. http://dx.doi.org/10.1093/nar/14.11.4683

Voss, M., B. Schröder, and R. Fluhrer. 2013. Mechanism, specificity, and physiology of signal peptide peptidase (SPP) and SPP-like proteases. *Biochim. Biophys. Acta*. 1828:2828–2839. http://dx.doi.org/10.1016/j.bbamem.2013.03.033

Weihofen, A., K. Binns, M.K. Lemberg, K. Ashman, and B. Martoglio. 2002. Identification of signal peptide peptidase, a presenilin-type aspartic protease. *Science*. 296:2215–2218. http://dx.doi.org/10.1126/science.1070925

Wiertz, E.J., T.R. Jones, L. Sun, M. Bogyo, H.J. Geuze, and H.L. Ploegh. 1996a. The human cytomegalovirus US11 gene product dislocates MHC class I heavy chains from the endoplasmic reticulum to the cytosol. *Cell*. 84:769–779. http://dx.doi.org/10.1016/S0092-8674(00)81054-5

Wiertz, E.J., D. Tortorella, M. Bogyo, J. Yu, W. Mothes, T.R. Jones, T.A. Rapoport, and H.L. Ploegh. 1996b. Sec61-mediated transfer of a membrane protein from the endoplasmic reticulum to the proteasome for destruction. *Nature*. 384:432–438. http://dx.doi.org/10.1038/384432a0

Yamaguchi, A., O. Hori, D.M. Stern, E. Hartmann, S. Ogawa, and M. Tohyama. 1999. Stress-associated endoplasmic reticulum protein 1 (SERP1)/Ribosome-associated membrane protein 4 (RAMP4) stabilizes membrane proteins during stress and facilitates subsequent glycosylation. *J. Cell Biol.* 147:1195–1204. http://dx.doi.org/10.1083/jcb.147.6.1195

Yang, Z.Z., and A.P. Zou. 2001. Transcriptional regulation of heme oxygenases by HIF-1alpha in renal medullary interstitial cells. *Am. J. Physiol. Renal Physiol.* 281:F900–F908.

Zettl, M., C. Adrain, K. Strisovsky, V. Lastun, and M. Freeman. 2011. Rhomboid family pseudoproteases use the ER quality control machinery to regulate intercellular signaling. *Cell*. 145:79–91. http://dx.doi.org/10.1016/j.cell.2011.02.047